

**Optoelectronic Oscillators and Their  
Applications to 60-GHz Fiber-Fed  
Wireless Systems**

**Kwang-Hyun Lee**

**THE GRADUATE SCHOOL**

**YONSEI UNIVERSITY**

**Department of Electrical and Electronic Engineering**

**Optoelectronic Oscillators and Their  
Applications to 60-GHz Fiber-Fed  
Wireless Systems**

by

*Kwang-Hyun Lee*

Submitted to the Department of Electrical and Electronic Engineering  
in partial fulfillment of the requirements for the degree of

**Doctor of Philosophy**

at the

**THE GRADUATE SCHOOL  
YONSEI UNIVERSITY**

**January 2008**

This certifies that the dissertation of Kwang-Hyun Lee is approved.

---

**Thesis Supervisor: Woo-Young Choi**

---

**Sang-Kook Han**

---

**Yongshik Lee**

---

**Jinwook Burm**

---

**Hyuk-Kee Sung**

**THE GRADUATE SCHOOL**

**YONSEI UNIVERSITY**

**January 2008**

# Table of Contents

<i>ABSTRACT</i> .....	xi
<b>1. INTRODUCTION</b> .....	1
1-1. RF oscillators .....	1
1-1-1. <i>General considerations</i> .....	1
1-1-2. <i>Oscillator phase noise limited by resonator's <math>Q</math></i> .....	4
1-2. Optoelectronic oscillators .....	9
1-2-1. <i>Operation principle of OEOs</i> .....	9
1-2-2. <i>Single-mode oscillation in OEOs</i> .....	14
1-3. Outline of dissertation.....	15
<b>2. CONVENTIONAL OPTOELECTRONIC OSCILLATORS</b> .....	17
2-1. Introduction.....	17
2-2. Optoelectronic oscillator with high- $Q$ BPF .....	18
2-3. Dual-loop optoelectronic oscillator .....	21
2-4. Injection-locked optoelectronic oscillator.....	25
2-4. Summary.....	28
<b>3. SINGLE-MODE EXTRACTION USING INJECTION-LOCKING IN OPTOELECTRONIC OSCILLATORS</b> .....	30
3-1. Introduction.....	30
3-2. Proposed scheme and operation principle.....	31
3-3. Experimental setup and results .....	34
3-4. Conclusion .....	43
<b>4. OPTOELECTRONIC SELF-INJECTION-LOCKED OSCILLATOR</b> .....	44
4-1. Introduction.....	44

4-2. Conventional SIL oscillator .....	45
4-2-1. Phase noise of SIL oscillators .....	46
4-2-2. Phase noise of the SIL oscillator having a long delay-line in the feedback route .....	49
4-2-3. Phase noise of the SIL oscillator having a high-Q resonator in the feedback route .....	51
4-3. Proposed SIL oscillator .....	53
4-3-1. Motivation .....	53
4-3-2. Proposed scheme and operation principle .....	55
4-3-3. Experimental setup and results .....	58
4-3-4. Summary .....	58
4-4. Compact and low-cost configuration for an optoelectronic SIL oscillator .....	66
4-4-1. Motivation .....	66
4-4-2. Proposed configuration for an optoelectronic SIL oscillator .....	67
4-4-3. Operation principle .....	69
4-4-4. Experimental setup and results .....	73
4-4-5. Summary .....	83
4-5. Conclusion .....	84

**5. 60-GHZ FIBER-FED WIRELESS SYSTEMS BASED ON OPTOELECTRONIC**

<b>SIL OSCILLATORS .....</b>	<b>86</b>
5-1. Introduction .....	86
5-1-1. Great interest in 60 GHz .....	87
4-4-1. 60-GHz fiber-fed wireless systems .....	89
5-2. Fiber-fed wireless system based on an optoelectronic SIL oscillator ..	93
5-2-1. Operation principle of LO signal generation and up-conversion ..	93
5-2-2. Experimental results for LO signal generation .....	96
5-2-3. Demonstration of data transmission along fiber and 60-GHz wireless links .....	101
5-3. Conclusion .....	108

<b>6. SUMMARY .....</b>	<b>110</b>
<b>BIBLIOGRAPHY.....</b>	<b>114</b>
<b>PUBLICATION LISTS .....</b>	<b>118</b>

## List of Figures and Tables

Fig.1-1. (a) Conceptual diagram for feedback oscillatory system. (b) Addition of a resonator to (a).....	3
Fig.1-2. Ideal <i>RLC</i> oscillator model.....	7
Fig.1-3. Phase-noise spectra: <i>Lesson's</i> model versus Eq. (1.6).....	7
Fig.1-4. (from [4]) $f \times Q$ according to the resonant frequency of several kinds of resonators. SAW and BAW mean surface acoustic wave and bulk acoustic wave, respectively.....	8
Fig.1-5. (a) Van der Pol oscillator. (b) Optoelectronic oscillator (OEO). .....	12
Fig.1-6. Detailed structure of an OEO. ....	13
Fig.1-7. Illustration of multimode oscillation in an OEO. ....	13
Fig.2-1. (a) Configuration of an OEO including a high-Q BPF for single-mode oscillation. (b) Illustration of multimode oscillation and the BPF response in an OEO. ....	20
Fig.2-2. Basic configuration of a typical dual-loop OEO. ....	23
Fig.2-3. Conceptual spectra of (a) long loop alone, (b) short-loop alone, and (c) both-loop closed.....	24
Fig.2-4. Block diagram of an injection-locked dual OEO. ....	27
Fig.3-1. Setup for demonstration of single-mode extraction from OEO modes and output spectra from different oscillators. ....	33
Fig.3-2. Experimental setup for demonstration of single-mode extraction from OEO modes.....	37
Fig.3-3. Measured locking range of the electrical oscillator according to the injection power.....	38

Fig.3-4. Measured output spectra of (a) electrical oscillator, (b) OEO having 2.4-km long SMF, and (c) injection-locked oscillator. The center frequencies are 30.0092985 GHz, 30.0071960 GHz, and 30.0092985 GHz, respectively.	39
Fig.3-5. Measured phase noises of output signals from the electrical and injection-locked oscillator, and OEO.	40
Fig.3-6. Measured spectra of different OEO modes selected by tuning the phase shifter.	41
Fig.3-7. SSB phase noise values measured at 10-kHz frequency offset and the mode power for the selected modes.	42
Fig.4-1. Self-injection-locked oscillator.	45
Fig.4-2. Configurations of (a) a typical dual-loop OEO and (b) the proposed self-injection-locked oscillator having a long optical delay line.	57
Fig.4-3. Experimental setup for demonstration of optoelectronic self-injection-locked oscillator.	61
Fig.4-4. Measured RF spectra of the output signals at (a) $\kappa=0$ , (b) $\kappa\sim 1.6\times 10^{-3}$ , and (c) $\kappa\sim 2.5\times 10^{-1}$ . The center frequencies are 29.9773362 GHz, 29.9770507 GHz, and 29.9768307 GHz, respectively. In all figures, the frequency span and resolution bandwidth settings were 300 kHz and 300 Hz, respectively.	62
Fig.4-5. Measured phase noises of the output signals at (a) $\kappa=0$ , (b) $\kappa\sim 1.6\times 10^{-3}$ , and (c) $\kappa\sim 2.5\times 10^{-1}$ .	63
Fig.4-6. SSB phase noises at 10-kHz frequency offset from the center frequency and SMSR according to the injection power level.	64
Fig.4-7. Compact and low cost configuration for an optoelectronic SIL oscillator based on a monolithic HPT oscillator and low cost optical components.	68
Fig.4-8. E/O converter and schematic optical spectra. The shade region means	

the gain wavelength range of LD2 and $\lambda_{LD2}$ is the wavelength of LD2 without any optical injection.....	72
Fig.4-9. Experimental setup for demonstration of a new configuration for an optoelectronic SIL oscillator.....	77
Fig.4-10. Schematic and photograph (from [26]) of HPT based monolithic oscillator.....	78
Fig.4-11. Measured optical spectra of the output signals from (a) the DFB LD directly modulated by the HPT-oscillator-output signal and (b) the FP LD with optical injection of the modulated output signals. ....	79
Fig.4-12. Measured RF spectra of the output signals for (a) no optical signal injection, (b) $P_{opt} = -6$ dBm, (c) $P_{opt} = 8$ dBm. The center frequencies are 10.790847 GHz, 10.790693 GHz and 10.790314 GHz, respectively. In all figures, the frequency span and resolution bandwidth settings were 1 MHz and 10 kHz, respectively.....	80
Fig.4-13. SSB phase noises at 10-kHz frequency offset from the center frequency according to the injection optical power level. ....	81
Fig.4-14. Measured phase noises of the optoelectronic output signals at different injection optical power values.....	82
Fig.5-1. Simple configuration for fiber-fed wireless systems.....	91
Fig.5-2. Advantages of fiber-fed wireless systems. ....	92
Fig.5-3. 60-GHz fiber-fed wireless system based on an optoelectronic SIL oscillator.....	95
Fig.5-4. Measured optical spectra of output signals from (a) directly modulated DFB LD and (b) the second DFB LD with optical injection of the modulated optical signals. ....	98
Fig.5-5. Generated 1 <sup>st</sup> and 2 <sup>nd</sup> harmonic LO signals according to the self-	

injection power level ( $\kappa$ ).....	99
Fig.5-6. Measured phase noises of 1 <sup>st</sup> (30 GHz) and 2 <sup>nd</sup> (60 GHz) LO signals with increasing self-injection power level ( $\kappa$ ). .....	103
Fig.5-7. 5MS/s 8-PSK data signals up-converted to the 60-GHz band.....	104
Fig.5-8. Constellation and eye diagram of the demodulated 5 MS/s 8-PSK data signals. ....	105
Fig.5-9. Measured constellation and eye diagram of the demodulated 5 MS/s 8-PSK data signals according to the self-injection power level ( $\kappa$ ). .....	106
Fig.5-10. Measured EVM of the demodulated 5 MS/s 8-PSK data signals as a function of self-injection power level ( $\kappa$ ). .....	107
Fig.5-11. Simple fiber-fed wireless system based on an optoelectronic SIL oscillator.....	109
Table 2-1. Comparison to previous OEOs.....	29

## Abstract

Two optoelectronic oscillators (OEOs) for generation of low phase-noise signals are proposed and experimentally demonstrated at millimeter-wave bands, and a 60-GHz fiber-fed wireless system based on the proposed OEO is introduced.

Firstly, a single-mode OEO is realized using an injection-locking method. The OEO consists of two oscillators, one of them is a single-loop OEO (a master oscillator) and the other is a typical electrical oscillator made up of an amplifier and a resonator (a slave oscillator). In the proposed scheme, the single mode is extracted from multiple OEO modes by injecting them into an electrical oscillator. One of the injected modes locks the electrical oscillator, while other modes are suppressed due to destructive interference in the electrical oscillator, resulting in single-mode oscillation. Although the phase noise is degraded about 6 dB at 10-kHz frequency offset by injection locking, extraction of a desired OEO mode among injected OEO modes separated by about 84 kHz at 30-GHz bands can be successfully demonstrated. However, the proposed scheme cannot produce the optical signal modulated by the generated low phase-noise electrical signal since an electrical oscillator is used as the slave oscillator.

In order to solve the above problem, an optoelectronic self-injection-locked (SIL) oscillator is proposed. In the SIL oscillator, a part of the electrical output signal is self-injected after passing through a long optical delay line for output phase-noise reduction. By controlling self-injection power, 30-GHz oscillation with side-mode suppression ratio (SMSR) larger than 50 dB and about 18-dB phase-noise reduction at 10-kHz frequency offset is demonstrated. Moreover, a compact and cost-effective configuration for the SIL oscillator, which is based on InP HPT-based monolithic oscillator and an electrical-to-optical converter composed of two low-speed laser diodes, is proposed and demonstrated at 10-GHz bands.

Finally, a 60-GHz fiber-fed wireless system is realized by using the optoelectronic SIL oscillator. In the system, the optoelectronic SIL oscillator performs local oscillator (LO) signal generation and all optical up-conversion, simultaneously. 5MS/s 8-PSK data signals are successfully transmitted along 10-km fiber-optic and about 1.5-m 60-GHz wireless links. In addition, the system performance depending on the phase noise of a LO signal is investigated.

Although this dissertation only introduces the fiber-fed wireless system as one of practical applications, the proposed OEO is very useful for the other photonic applications since it can simultaneously

generate optical signals as well as micro-/millimeter wave signals.

---

**Keywords:** Optoelectronic oscillators (OEO), Phase noise, Self-injection locked (SIL) oscillators, Micro-/millimeter waves, Injection-locking technique, 60 GHz, Fiber-fed wireless systems.

**STUDENT NUMBER: 10320197**

# Chapter 1

## Introduction

### 1-1. RF oscillators

#### *1-1-1. General considerations*

Oscillators are one of key components required in all modern radar and wireless communication systems to perform carrier generation and frequency up/down conversion. They produce a sinusoidal steady-state RF signal from DC power with a self-sustaining mechanism where the noise grows and finally becomes a periodic signal.

Their basic conceptual operation can be viewed as the linear feedback circuit shown in Fig. 1-1 (a) [1, 2]. The overall transfer function can be expressed as

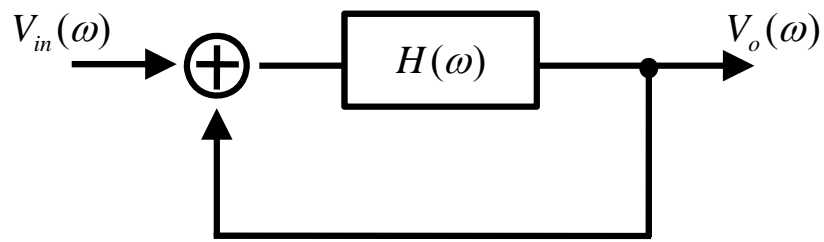
$$\frac{V_o(\omega)}{V_{in}(\omega)} = \frac{H(\omega)}{1 - H(\omega)}. \quad (1.1)$$

If the denominator of (1.1) becomes zero at a particular frequency, a self-sustaining mechanism works and non-zero output can be achieved

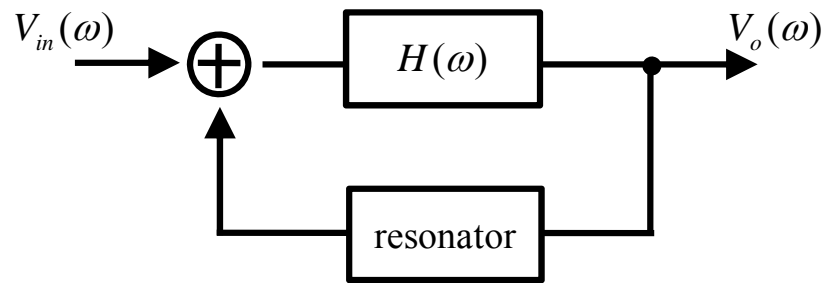
with a zero input. For steady-state oscillation, the operation condition must be satisfied with following two conditions at the oscillation frequency:

- The loop gain must be equal to unity
- The total loop phase shift must be equal to zero

The above conditions mean that any feedback system can oscillate if its loop gain and loop phase are properly controlled as can be seen in Fig. 1-1 (a). Ring oscillators and phase shift oscillators are examples. However, most RF oscillators have a frequency-selective network, called a resonator, in order to stabilize the oscillation frequency shown in Fig. 1-1 (b).



(a)



(b)

Fig.1-1. (a) Conceptual diagram for feedback oscillatory system. (b) Addition of a resonator to (a).

### ***1-1-2. Oscillator phase noise limited by resonator's $Q$***

As other RF devices, amplitude and phase of an oscillator output are susceptible to noise injected by its constituent devices or by external noise sources. In most case, the amplitude noise can be negligible or unimportant since all practical oscillators have amplitude-limiting mechanism [3]. Thus, the key parameter describing the characteristics of an oscillator is phase noise of its output signal.

In case of an ideal oscillator shown in Fig. 1-2, which is composed of a lossy resonator and an energy restoration element, the single-side band noise spectral density can be expressed by

$$L\{\Delta\omega\} = 10 \cdot \log\left[\frac{2kT}{P_{sig}} \cdot \left(\frac{\omega_0}{2Q\Delta\omega}\right)^2\right] \quad (1.2)$$

where,  $\Delta\omega$  and  $\omega_0$  is the offset and oscillation frequency, respectively,  $Q$  is the quality factor of the unloaded  $LC$  tank, and  $P_{sig}$  is the oscillator output power [3].

From the equation (1.2), it can be known that the phase noise at a given offset frequency improves as both the output power and  $Q$  increases. It makes sense. Increasing output power reduces the phase noise because the thermal noise is fixed, while increasing  $Q$  also

induces the same effect because the tank impedance falls off as  $1/Q\Delta\omega$ .

However, there are big differences between the spectrum predicted by (1.2) and the measured spectrum due to additional important noise sources besides tank loss. For example, a practical energy restorer will be noisy. Moreover, measured spectra do not continue to drop quadratically, but finally flatten out at a large frequency offset due to the noise related to any active components placed between the tank and the outside world. Last, at very small offset frequency, measured spectra falls off as  $1/(\Delta\omega)^3$  because of the flicker noise.

In order to account for these discrepancies, Leeson provided the modified formula expressed by [3]

$$L\{\Delta\omega\} = 10 \cdot \log\left[\frac{2FkT}{P_{sig}} \cdot \left\{1 + \left(\frac{\omega_0}{2Q\Delta\omega}\right)^2\right\} \left(1 + \frac{\omega_f^3}{|\Delta\omega|}\right)\right]. \quad (1.3)$$

This modified formula includes a factor  $F$  to explain the increased noise in the region where the phase noise is proportional to  $1/(\Delta\omega)^2$ , an additive factor of unity within the braces to account for the noise floor, and a multiplicative factor to give a  $1/(\Delta\omega)^3$  behavior at small frequency offsets. Fig. 1-3 shows the phase-noise spectra for an ideal

and Leeson's models.

Although Leeson's model can explain the phase-noise spectra more exactly than the ideal oscillator model, the fact that increasing  $Q$  and signal power are ways to improve phase noise still haven't changed. Therefore, the highest  $Q$  produces the lowest phase noise.

Many types of high- $Q$  resonators have been proposed and demonstrated [4] and Fig. 1-4 compares the performance of several types of acoustic and electromagnetic resonators in terms of  $f \times Q$  ( $f$ : resonant frequency) figure of merit according to the resonant frequency.

Among them, acoustic based resonators based on quartz crystals are extremely attractive at MHz range owing to the small size, but they are lossy at microwave frequencies. On the other hand, dielectric resonators (DRs) realized with materials having high relative dielectric constant can be used at high frequency bands. The highest figure of merit at microwave and millimeter-wave frequencies is obtained by super-conductor based resonators. However, it requires cryogenic coolers [4].

Therefore, it is not an easy task to generate low phase-noise signals at high frequency bands such as millimeter-waves with electrical resonators.

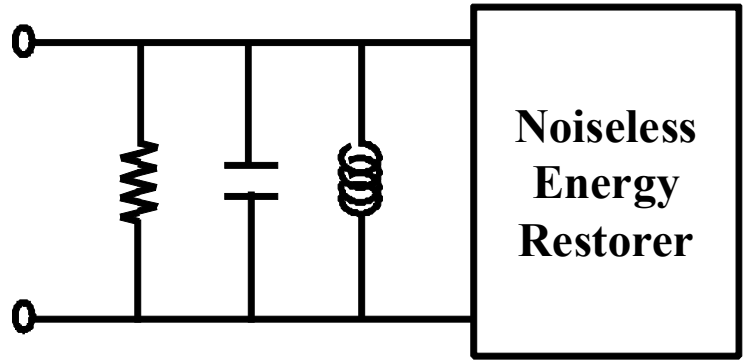


Fig.1-2. Ideal *RLC* oscillator model.

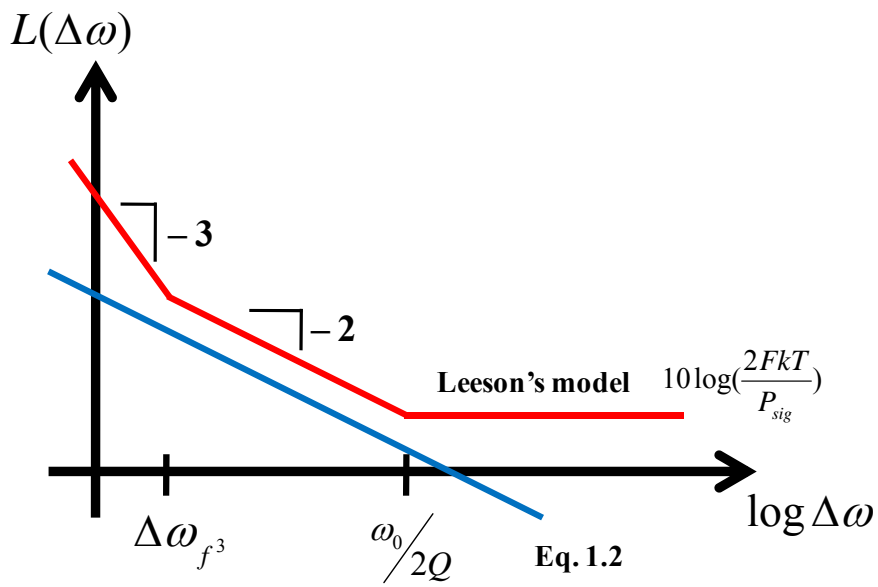


Fig.1-3. Phase-noise spectra: *Leeson's* model versus Eq. (1.2).

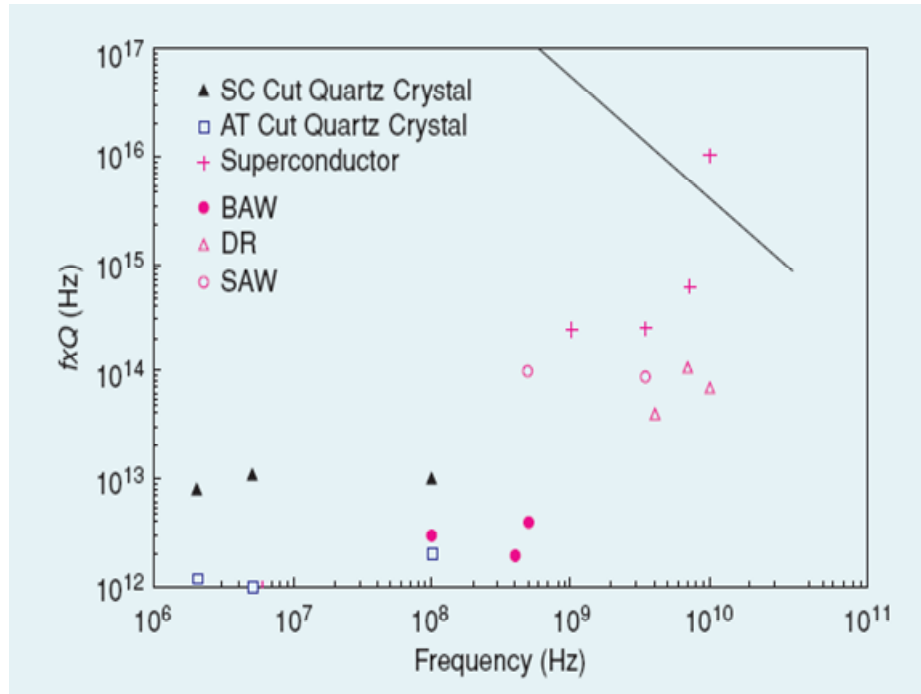


Fig.1-4. (from [4])  $f \times Q$  according to the resonant frequency of several kinds of resonators. SAW and BAW mean surface acoustic wave and bulk acoustic wave, respectively.

## 1-2. Optoelectronic oscillators

Unlike the previous acoustic or electromagnetic resonators, optical resonators based on an optical delay line potentially achieve ultra high- $Q$  even at millimeter-wave bands. This section will focus on basic theory of optoelectronic oscillators (OEOs) using optical delay lines as high- $Q$  external resonators and mention a critical issue in realizing OEOs.

### *1-2-1. Operation principle of OEOs*

Basically, the configuration of an OEO is similar to that of the van der Pol oscillator as shown in Fig. 1-5 [5]. In the van der Pol oscillator, the flux of electrons from the cathode to the anode is controlled by the potential on the intervening grid and this potential is affected by the feedback current in the anode circuit including an  $RLC$  network, as shown in Fig. 1-5 (a).

Fig. 1-5 (b) shows that the van der Pol oscillator can be converted to an OEO by replacing the function of electrons by photons, the function of the grid by an electrical-to-optical (E/O) converter, the function of the anode by an optical-to-electrical (O/E) converter, and finally the

energy-storage function of the  $LC$  circuit by a long optical delay line. Namely, the oscillator converts the continuous light energy to an RF signal, thus it was referred ‘optoelectronic oscillator’.

The more detailed construction of an OEO is described in Fig. 1-6. In this depiction, light from an E/O modulator is detected by a photo detector after passing through a long optical delay line and then it is amplified and fed back to the electrical port of the E/O modulator. If the modulator is properly biased and the small-signal loop gain is larger than unity, self-sustained oscillations are achieved [6, 7].

Once the feedback loop has the loop gain larger than unity, the OEO generates equally spaced peaks (or called modes) similar to that of a Fabry-Perot resonator, as shown in Fig. 1-7. The mode spacing is determined by  $c/nL$ , where  $c$  is the light speed,  $n$  is the fiber refractive index, and  $L$  is the loop length.

The power-spectral density of the each mode is found to be

$$S_{RF}(f) = \frac{\rho_N G_A^2 / P_{OSC}}{(\delta / 2\tau)^2 + (2\pi)^2 (\tau f)^2} \quad (1.4)$$

where  $f$  is the frequency offset from the oscillation frequency,  $\tau$  is the loop delay time,  $\rho_N$  is the total noise density which is sum of the

detector noise density including thermal and shot noise and the laser's relative intensity noise density [5-7].

From (1.4), the phase noise of an OEO decreases quadratically with the frequency offset and it is inversely proportional to the square of loop-delay time at given offset frequency.

The quality factor  $Q$  of the oscillator from (1.4) is

$$Q = \frac{f_{osc}}{\Delta f_{FWHM}} = Q_D \frac{\tau}{\rho_N G_A^2 / P_{OSC}} \quad (1.5)$$

where  $Q_D (= 2\pi f_{osc} \tau)$  is the quality factor of the optical delay line and it has larger value with longer delay line. For example, 1-km optical-delay-line length can produce  $Q_D$  of  $\sim 10^6$  at 30 GHz.

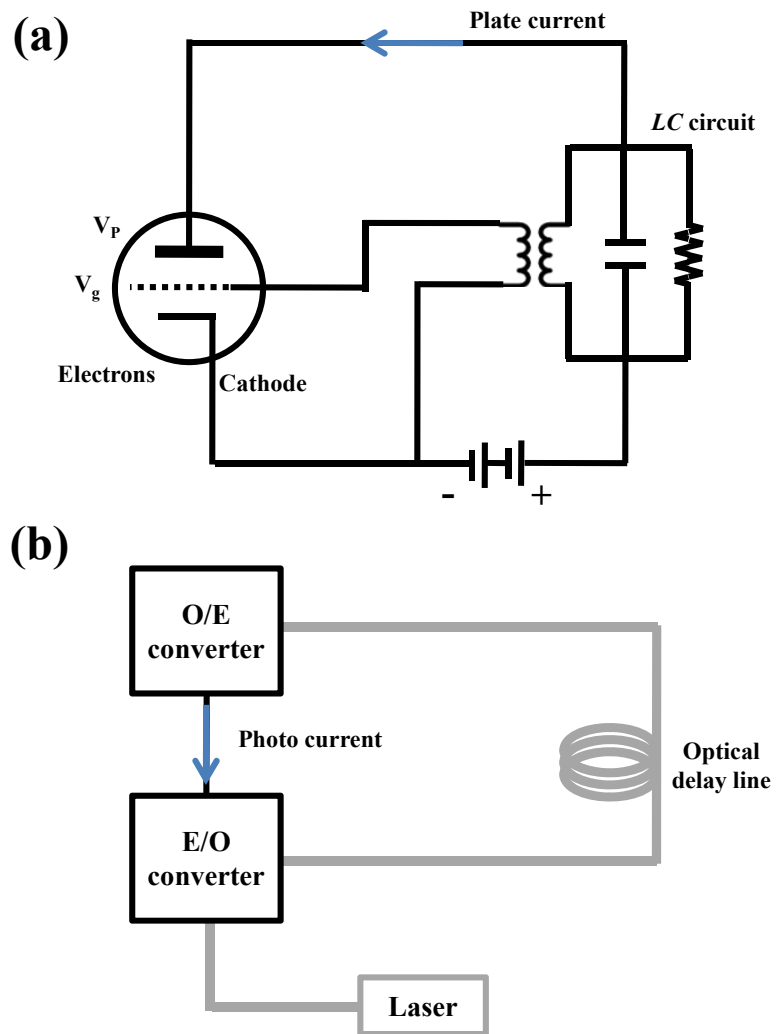


Fig.1-5. (a) Van der Pol oscillator. (b) Optoelectronic oscillator (OEO).

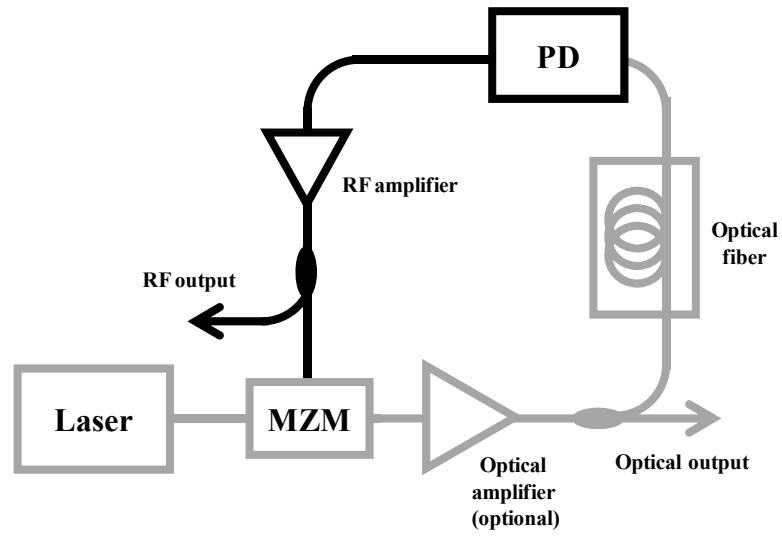


Fig.1-6. Detailed structure of an OEO.

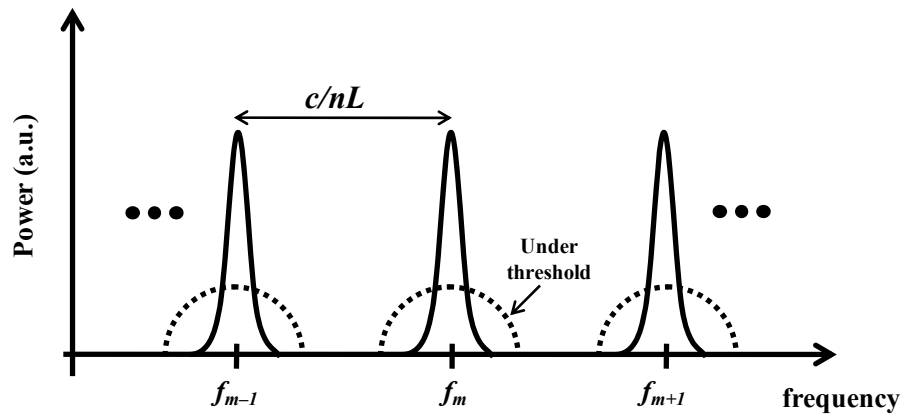


Fig.1-7. Illustration of multimode oscillation in an OEO.

### ***1-2-2.Single-mode oscillation in OEOs***

The main issue, in researching an OEO, is to realize single-mode oscillation. As mentioned in the previous section, the OEO generates multi modes which are equally spaced in a frequency domain and the mode spacing is inversely proportional to the loop length. Therefore, the lower phase noise is obtained with longer delay line but the mode-spacing is also reduced. For example, a few-km fiber length produces the mode spacing of several tens of kHz.

In most applications, the oscillator output should have a single mode as well as low phase-noise signal since the other oscillation modes degrade the system performance by reducing signal-to-noise ratio (SNR). In OEOs, single-mode oscillation can be achieved by inserting a high- $Q$  electrical band-pass filter (BPF) to the OEO loop but such high- $Q$  filters are hard to make at higher frequencies such as millimeter waves.

Therefore, the several optical methods have been used for realizing single-mode oscillation in the OEO and they will be discussed in chapter 2.

### **1-3. Outline of dissertation**

The main purpose of this dissertation is to propose new single-mode optoelectronic oscillators (OEOs) and to demonstrate 60-GHz fiber-fed wireless systems based on the proposed OEO. Details of dissertation outline are as follows.

In chapter 2, the conventional configurations for an OEO are discussed. Several kinds of studies have been proposed and demonstrated for single-mode oscillation in the OEO. The characteristic and performance of these previous works are compared with each other at chapter 2.

The new proposed configurations for an OEO are proposed and evaluated over the chapter 3 and 4. The chapter 3 proposes a hybrid injection-locked OEO, where a long-loop OEO injection locks an electrical oscillator. This scheme can successfully suppress the spur modes with a simple and cost-effective configuration, but it cannot generate the intensity-modulated optical signal contrary to the general OEO.

Chapter 4 introduces an optoelectronic self-injection locked (SIL) oscillator to generate an intensity-modulated optical carrier as well as a low phase-noise millimeter-wave signal. In the proposed oscillator, a

part of the output signal is self-injected into the oscillator itself after passing through a long optical delay line, resulting in oscillator locking and phase-noise reduction. By controlling the self-injection power, single-mode oscillation at 30-GHz band with SMSR larger than 50 dB and about 18-dB phase-noise reduction at 10-kHz frequency offset is achieved. In addition, the simpler and more cost effective configuration for the optoelectronic SIL oscillator will be presented. In the proposed scheme, the free-running oscillator is realized with an InP HPT-based monolithic oscillator and electrical-to-optical conversion is carried out by two low-speed and low-cost laser diodes. With this new configuration, more than 55-dB phase-noise reduction at 10-kHz frequency offset from the center frequency of about 10.8 GHz by injecting 8-dBm optical signals is demonstrated without using any high-speed optoelectronic components.

In chapter 5, a 60-GHz fiber-fed wireless system based on the proposed optoelectronic SIL oscillator is proposed and 5MS/s 8-PSK data transmission at a 60 GHz band is demonstrated. In addition, system performances are evaluated by measuring the error vector magnitude (EVM) value.

Finally, this dissertation will be summarized in chapter 6.

## **Chapter 2**

### **Conventional Optoelectronic Oscillators**

#### **2-1. Introduction**

In this chapter, the previously reported configurations for realization of an optoelectronic oscillator (OEO) are discussed and compared in detail. A great deal of effort has been expended to realize single-mode oscillation in multiple OEO modes. Following sections will introduce three conventional methods for realization of single-mode oscillation:

- By using an electrical band-pass filter
- By using dual optical loops having the different length
- By using injection locking method.

## 2-2. Optoelectronic oscillator with high-Q BPF

The simplest technique for single-mode oscillation is to insert an electrical band-pass filter (BPF) into the feedback loop. Fig. 2-1 (a) shows the configuration of an OEO including a BPF. The mode selection and side-mode suppression ratio (SMSR) defined as the power ratio between the oscillating mode and the side mode closest to the oscillating mode are determined by the BPF characteristics. The BPF's  $Q$  should be enough high to extract only the desired oscillation mode with high suppression of other modes, as shown in Fig. 2-1 (b) [8-10].

Many previous works have reported a single-mode OEO with this technique. For example, Yu ji *et al* presented single-mode oscillation by using a dielectric resonator having the external  $Q$  of  $\sim 5000$  at the center frequency of 9.56 GHz [8]. The optical delay-line which is a single-mode fiber had a length of about 6 km and they achieved the phase noise of -130 dBc/Hz at 10-kHz frequency offset with SMSR of about 50 dB. On the other hand, D. Eliyahu *et al.* achieved the phase noise of about -140 dBc/Hz at 10-kHz frequency offset from the center frequency of 8.98 GHz with SMSR of 90 dBc/Hz [9] with a homemade BPF having  $Q$  of 38,000.

Although, the previous results have been successfully demonstrated the single-mode oscillation with a high- $Q$  BPF, such high- $Q$  filters are not always available at low cost and harder to make at higher frequencies such as millimeter waves due to their ohmic and dispersive losses. In addition, this limitation in realizing high- $Q$  filters restricts the reduction of OEO's phase-noise by limiting the delay-line length. It is because that the longer delay line provides the lower phase noise, but it also induces the narrower frequency spacing between OEO modes. For example, a 1-km fiber length produces the mode spacing of 200 kHz, requiring a higher  $Q$  filter than  $\sim 10^5$  at the oscillation frequency of 30 GHz for single-mode oscillation. It is hard to make such high- $Q$  filters at millimeter-wave bands.

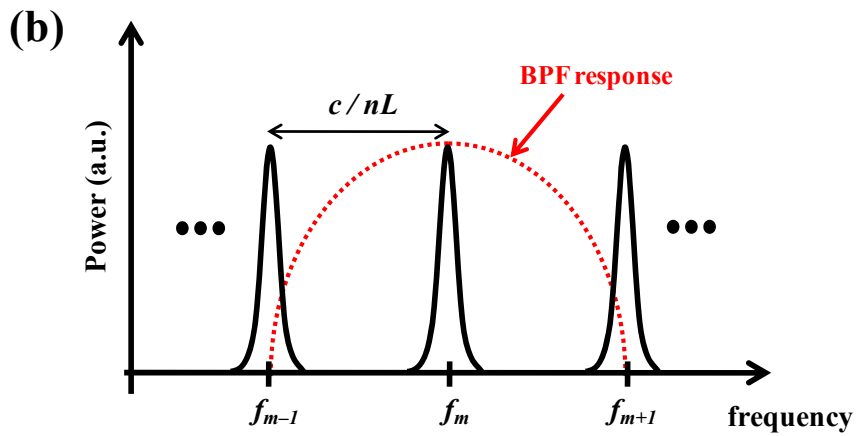
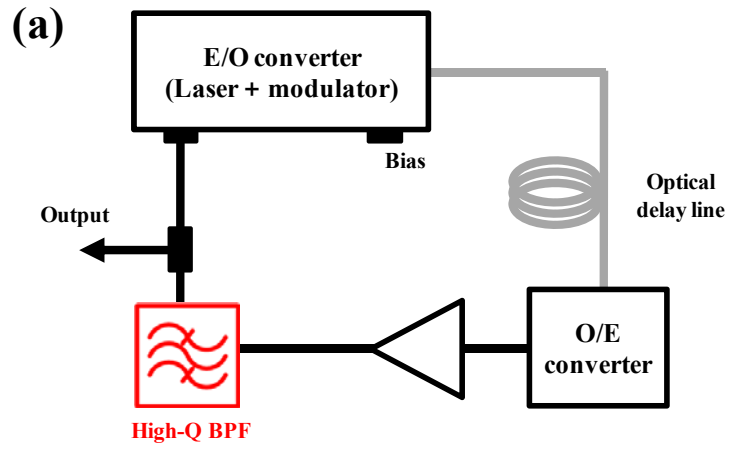


Fig.2-1. (a) Configuration of an OEO including a high-Q BPF for single-mode oscillation. (b) Illustration of multimode oscillation and the BPF response in an OEO.

### **2-3. Dual-loop optoelectronic oscillator**

Unlike the single-loop OEO requiring a high-Q BPF, a dual-loop OEO can achieve high-spectral-purity microwave signals without using a high-Q filter [9, 11]. Fig. 2-2 shows the basic configuration of a dual-loop OEO. As shown in the figure, the optical signal generated by an E/O converter is divided into two optical loops having a different length and converted electrical signals by an O/E converter. The two converted signals are amplified and coupled by an RF coupler and then fed to an RF port of the E/O converter. The operation of each loop is equivalent to a single-loop OEO, but mode selectivity is quite different.

In the dual-loop OEO, every mode of each loop cannot oscillate due to interferences between two combined signals at the RF coupler. Fig. 2-3 conceptually describes this effect. Most of the long-loop modes suffer high transmission loss by the short loop except the modes satisfying the phase-matching condition of the two loops at the same time. Therefore, the mode spacing is determined by the short loop, while the phase noise is mainly determined by the long loop resulting in following advantages:

- Large mode spacing with low phase noise can be achieved.

- The large mode spacing determined by the short optical loop can reduce the  $Q$  of a BPF required for single-mode oscillation.
- The oscillation can be started with the each loop's small-signal gain of 0.5 since each loop shares the loop gain.

With this OEO, X. S. Yao *et al* successfully demonstrated single-mode oscillation at 10 GHz with -140 dBc/Hz at 10-kHz frequency offset and the obtained SMSR is more than 60 dB [11].

However, the increase of the SMSR in the dual-loop OEO is limited since two loops are coupled to each other. The side modes suppressed by the short loop are still supported by the long loop. Moreover, the high  $Q$  produced by the long loop is sacrificed by the short loop due to its parallel configuration [12].

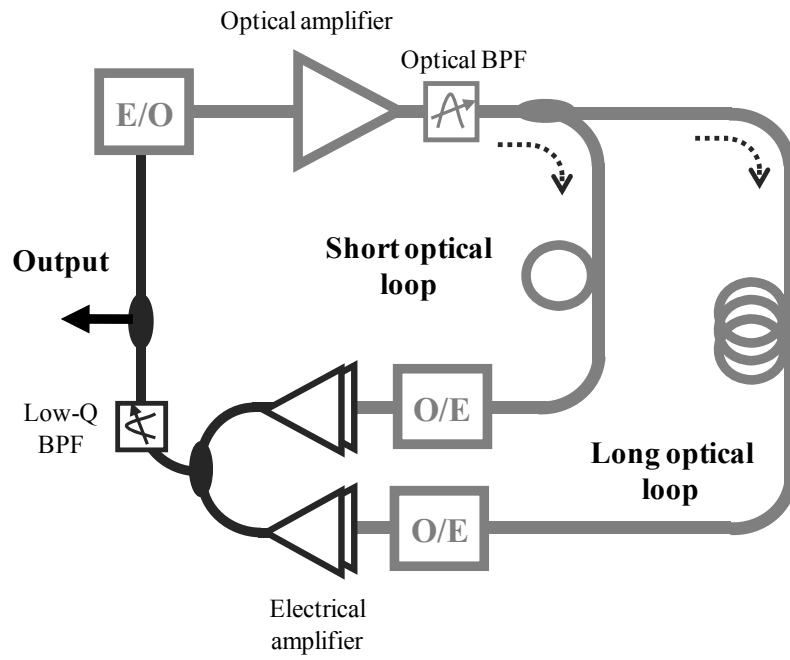


Fig.2-2. Basic configuration of a typical dual-loop OEO.

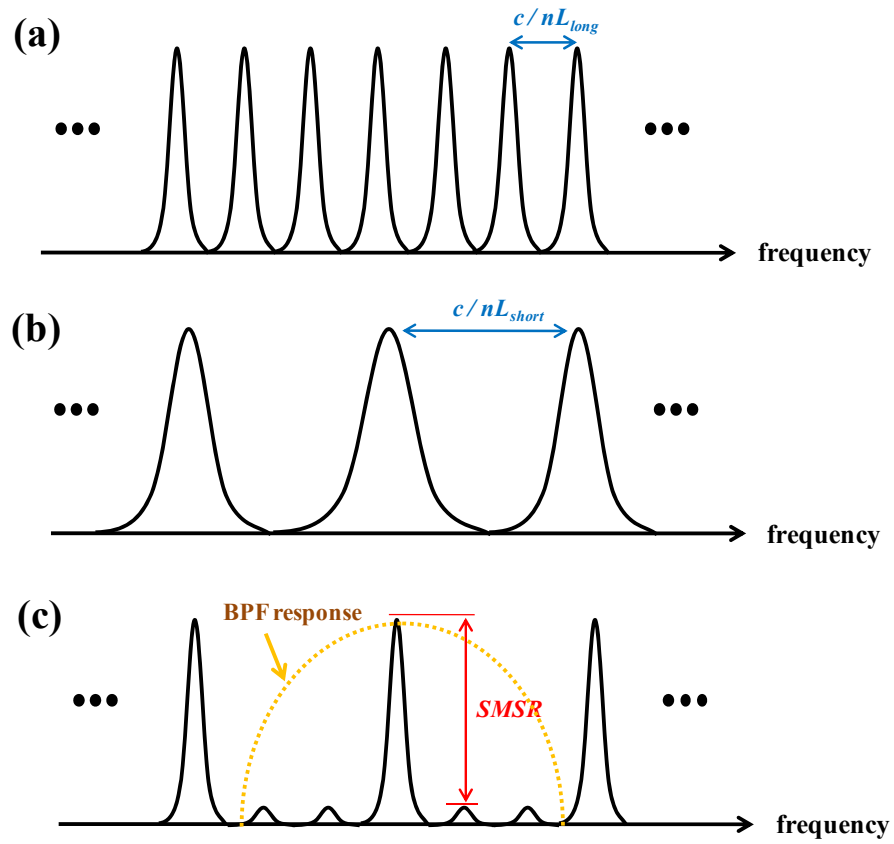


Fig.2-3. Conceptual spectra of (a) long loop alone, (b) short-loop alone, and (c) both-loop closed.

### 2-3. Injection-locked optoelectronic oscillator

In order to obtain the high SMSR without sacrificing high- $Q$  characteristic generated by a long optical loop, Weimin Zhou *et al* introduced an injection-locked OEO in 2005 [12].

Injection locking schemes have been proposed and demonstrated the phase-noise improvement of low- $Q$  slave oscillators with a high- $Q$  master oscillator in RF domain [13, 14]. On the other hand, the injection-locked OEO used the injection locking scheme to filter out the multiple side modes in the high- $Q$  master OEO by injecting the OEO modes into a slave OEO.

Fig. 2-4 shows the block diagram of an injection-locked OEO. As shown in the figure, RF output signals from a long-loop master OEO are injected into a short-loop OEO. The loop length and BPF's  $Q$  in the slave OEO should be precisely designed such that only one mode is oscillated.

Once the multiple OEO modes are injected into the slave OEO, the one of injected OEO modes, which is closest to the slave mode in frequency domain, injection locks the slave mode, while the injected other modes are drastically suppressed due to their destructive interference experienced in the slave OEO [12].

By using this injection-locking technique, [12] achieved the phase noise of about -150 dBc/Hz at 10-kHz offset frequency from the center frequency of 10 GHz as well as the SMSR of 140 dBc/Hz.

However, it is difficult to lock the short-loop slave OEO with output RF signals from the master OEO due to its narrow locking range especially at millimeter-wave bands. The frequency of the injected signal should be fine-tuned or the large injection power is needed to increase the locking range. Moreover, the number of high-speed optical and electrical components is doubled for realizing two OEOs.

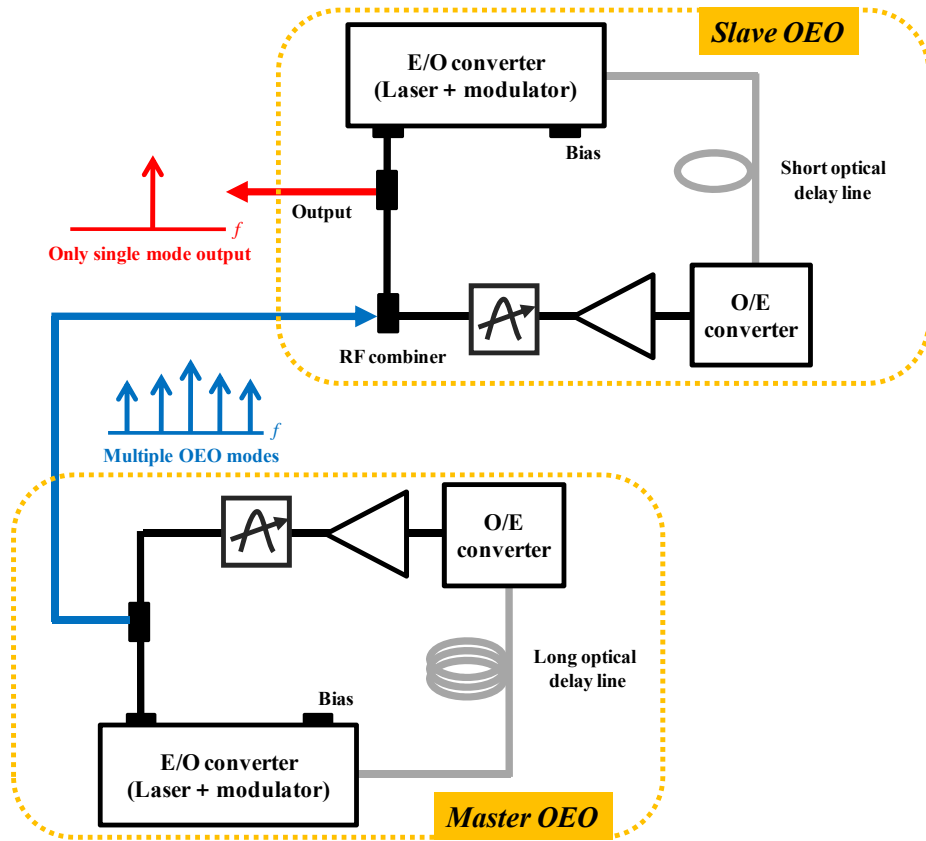


Fig.2-4. Block diagram of an injection-locked dual OEO.

## 2-4. Summary

In Table 2-1, three conventional OEOs as discussed in the previous section are summarized and compared to each other.

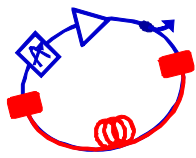
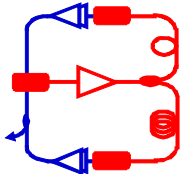
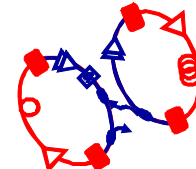
By simply inserting a high- $Q$  band-pass filter (BPF) into the feedback loop in an OEO, single-mode oscillation can be easily achieved, but the limited  $Q$  of the BPF restrict the increase of the loop length, limiting the phase-noise improvement.

On the other hand, a dual-loop OEO can achieve single-mode oscillation with relatively low- $Q$  BPF. It can provide low phase noise with a long loop and the high SMSR with a short loop. However, the increase of SMSR is limited since two loops are coupled to each other.

In order to further increase the SMSR, an injection-locked dual-loop OEO, where a long-loop OEO injection-locks a short-loop single-mode OEO, has been proposed. This method can achieve very high SMSR, but it is hard to lock the short-loop OEO due to its narrow locking range. Moreover, its configuration is complex and expensive since the number of high-speed optical and electrical components is doubled for realizing two OEOs.

In the next chapter 3 and 4, new configurations for an OEO are proposed and experimentally demonstrated.

Table 2-1. Comparison to previous OEOs.

	Configuration	SMSR	Phase noise	Note
Single-loop OEO		Very poor	Excellent	✓ Multimode oscillation
Dual-loop OEO		Good	Good	<ul style="list-style-type: none"> <li>✓ Coupled two loops</li> <li>- Average <math>Q</math></li> <li>- Limited SMSR</li> <li>✓ Two O/E converters</li> </ul>
Injection-locked OEO		Excellent	Very good	<ul style="list-style-type: none"> <li>✓ Two OEOs</li> <li>✓ Sensitive operating conditions</li> </ul>

## **Chapter 3**

# **Single-Mode Extraction Using Injection-Locking in Optoelectronic Oscillators**

### **3-1. Introduction**

In this section, an injection-locked OEO different from the OEO discussed in chapter 2 is proposed for single-mode extraction. Unlike the previously injection-locked OEO, the slave short-loop OEO is replaced with an electrical oscillator, resulting in a simple and cost-effective configuration [15].

In the proposed scheme, the electrical oscillator works as a high- $Q$  band-pass filter (BPF) for selecting a single mode from the injected OEO modes. The stable injection locking can be achieved with the low injection power due to its wider locking range compared with an OEO. As demonstration of the proposed scheme, a single mode is extracted from multiple OEO modes having about 84-kHz mode spacing at 30-GHz bands.

### 3-2. Proposed scheme and operation principle

Fig. 3-1 conceptually shows the setup for demonstrating single-mode extraction from multiple OEO modes along with output spectra of optoelectronic and electrical oscillators. It is assumed that both oscillators have sufficient gain for self-oscillation. Once multiple OEO modes are injected into the electrical oscillator, the mode closest to the electrical-loop mode injection-locks the electrical mode and other modes are drastically suppressed due to the destructive interference in the electrical loop [12]. For stable injection-locking, the power of the injected OEO modes should be limited so that the locking range becomes narrower than the half of the OEO-mode separation, called the free-spectral range (FSR).

The locking range ( $\Delta f$ ) can be expressed by

$$\Delta f \approx \frac{f_0}{2Q} \sqrt{\frac{P_{in}}{P_{out}}} \quad (3.1)$$

where  $f_0$  is the oscillation frequency,  $Q$  is the quality factor of the band-pass filter (BPF) inserted in the electrical loop, and  $P_{in}$  and  $P_{out}$  are injected and output signal power, respectively [16]. Therefore, the

injection power range for stable injection locking can be described as

$$P_{in} < P_{out} \left( \frac{FSR}{2} \cdot \frac{2Q}{f_0} \right)^2. \quad (3.2)$$

If the injection power satisfies (3.2), only one mode can lock the electrical-loop mode.

The phase noise of the locked signal is given by

$$\varphi_{locked}(\omega) = \frac{\cos^2(\phi_0)}{\cos^2(\phi_0) + \left(\frac{\omega}{\Delta\omega}\right)^2} \varphi_{in}(\omega) + \frac{\left(\frac{\omega}{\Delta\omega}\right)^2}{\cos^2(\phi_0) + \left(\frac{\omega}{\Delta\omega}\right)^2} \varphi_{free}(\omega) \quad (3.3)$$

where,  $\varphi_{in}(\omega)$  is the phase noise of the injected signal,  $\varphi_{free}(\omega)$  is the phase noise of the output signal from the electrical oscillator without signal injection,  $\phi_0$  is the constant phase difference between the injected and locked signal, and  $\omega$  is the offset frequency [17]. As  $\omega$  approaches zero, the phase noise of the locked signal approaches  $\varphi_{in}(\omega)$ . Therefore, single-mode selection from injected OEO modes can be realized with small phase-noise degradation near the oscillation frequency.

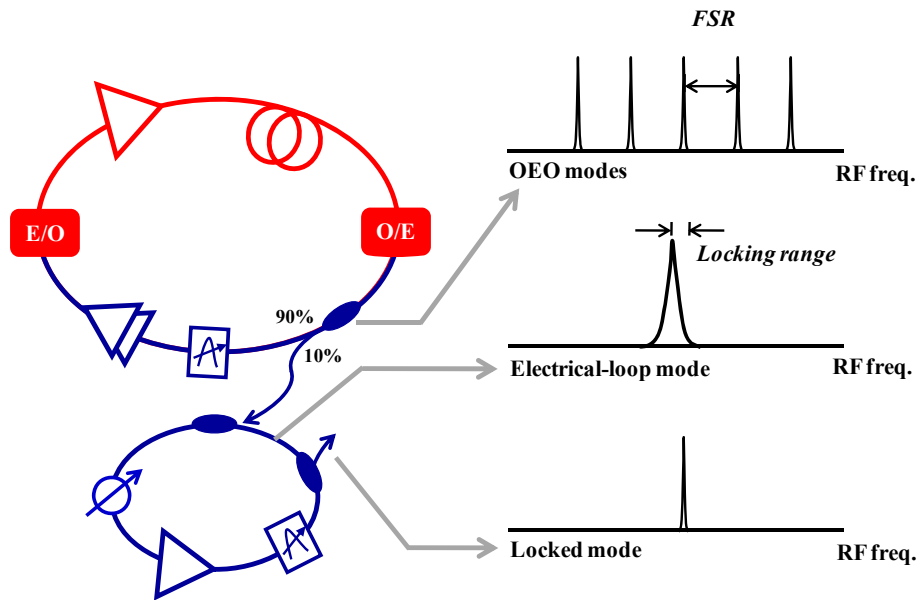


Fig.3-1. Setup for demonstration of single-mode extraction from OEO modes and output spectra from different oscillators.

### 3-3. Experimental setup and results

Fig. 3-2 shows the experimental setup for demonstration of the proposed scheme. As shown in Fig. 3-2, the electrical oscillator was composed of an electrical amplifier having RF gain of about 18 dB, an RF filter having  $Q$  of 1000 at 30 GHz with 3.16-dB insertion loss, a 4-port 3-dB RF coupler for signal injection and extraction, and a phase shifter for tuning the oscillation frequency.

First of all, the locking range of the electrical oscillator was measured according to the injection power to obtain the injection-power range for stable injection-locking and the results are shown in Fig. 3-3. The figure indicates that the injection power should be lower than about  $-39$  dBm to keep the locking range under the FSR of 84 kHz induced by the 2.4-km optical delay line. In the demonstration, the injection power was set  $-42$  dBm.

Fig. 3-4 (a) and (b) show the output spectrum of the electrical oscillator and the OEO, respectively, while Fig. 3-4 (c) shows the injection-locked output spectrum. They were measured by an RF spectrum analyzer (HP8563E) connected with an external mixer (HP11970A) after attenuation about 9 dB due to the display limit of the spectrum analyzer. For all three measurements, the frequency span and

the resolution bandwidth was set 300 kHz and 300 Hz, respectively.

The power difference between modes, shown in Fig. 3-4 (b), is due to the gain competition between OEO modes. As shown in the figures, the injected OEO modes are drastically suppressed except the only one OEO mode locking the electrical oscillator and the signal quality of the locked mode follows that of the injected OEO mode.

In order to investigate the signal quality, the single-sideband (SSB) phase noises of output signals from the electrical, optoelectronic and injection-locked oscillator were measured at the frequency offset from 3 kHz to 100 kHz and the results are shown in Fig. 3-5. As can be seen in the figure, the injection-locked signal has higher phase noises than the injected OEO mode around 10-kHz frequency offset. It is because that the phase noise of the electrical oscillator itself affects that of the locked signal as shown in Eq. (3.3). However, it is believed that the phase-noise degradation is reduced as the offset frequency approaches zero.

The measured phase-noise values of the injected and locked signal at 10-kHz frequency offset are -118.83 dBc/Hz and -112.00 dBc/Hz, respectively. Although injection-locking induces the phase-noise degradation of about 6 dB at 10-kHz frequency offset, it can drastically suppress side modes. The phase-noise peaking at ~20-kHz frequency

offset is believed due to our measurement setup using an external mixer.

If the oscillation frequency of the electrical oscillator is changed by tuning the phase shifter, other OEO modes can be selected and the results are shown in Fig. 3.6. They were obtained under the same experimental condition for Fig. 3.4 (c) except the phase change in the electrical oscillator. Fig. 3.6 (a) and (b) show the selected OEO mode located at just left and right side from the selected mode shown in Fig. 3.4 (c), respectively.

Fig. 3.7 shows the selected mode's power and phase noise measured at 10-kHz frequency offset while tuning the phase shifter. In the figure, the mode having oscillation frequency of 30.754892 GHz is set the 0<sup>th</sup> mode, and the mode number increases (and decreases) for each mode having 84-KHz offset.

In this demonstration, more than 150 modes were chosen with the constant mode power and phase noise. As shown, the desired OEO mode can be extracted by simply tuning the phase shifter in the electrical oscillator.

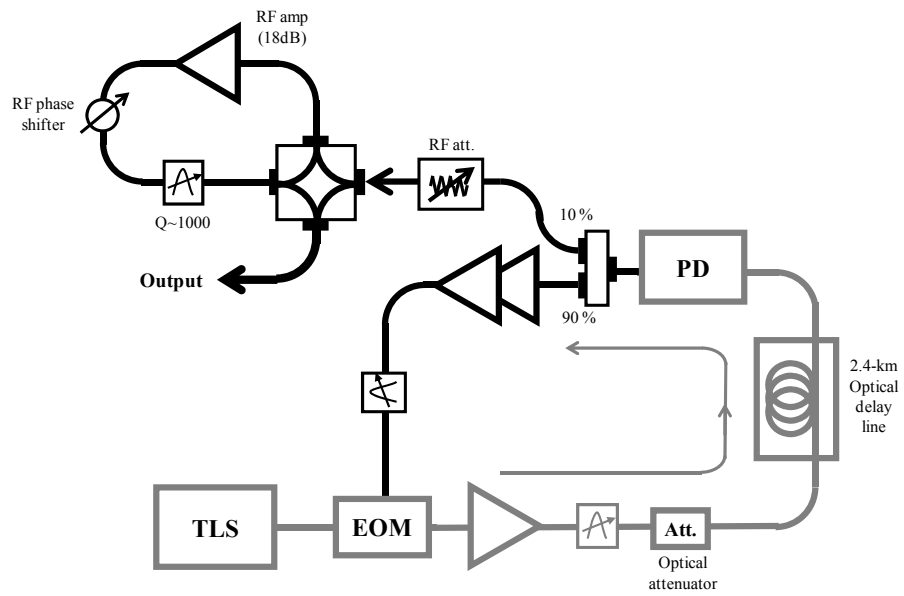


Fig.3-2. Experimental setup for demonstration of single-mode extraction from OEO modes.

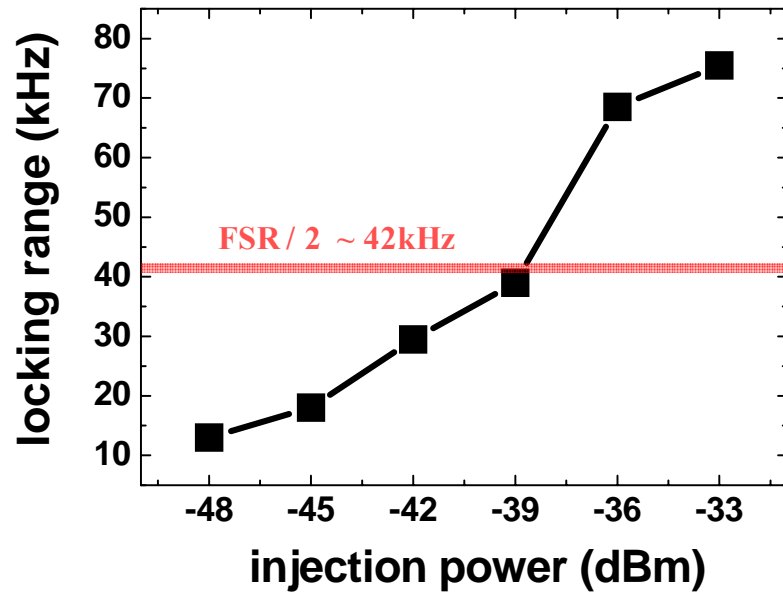


Fig.3-3. Measured locking range of the electrical oscillator according to the injection power.

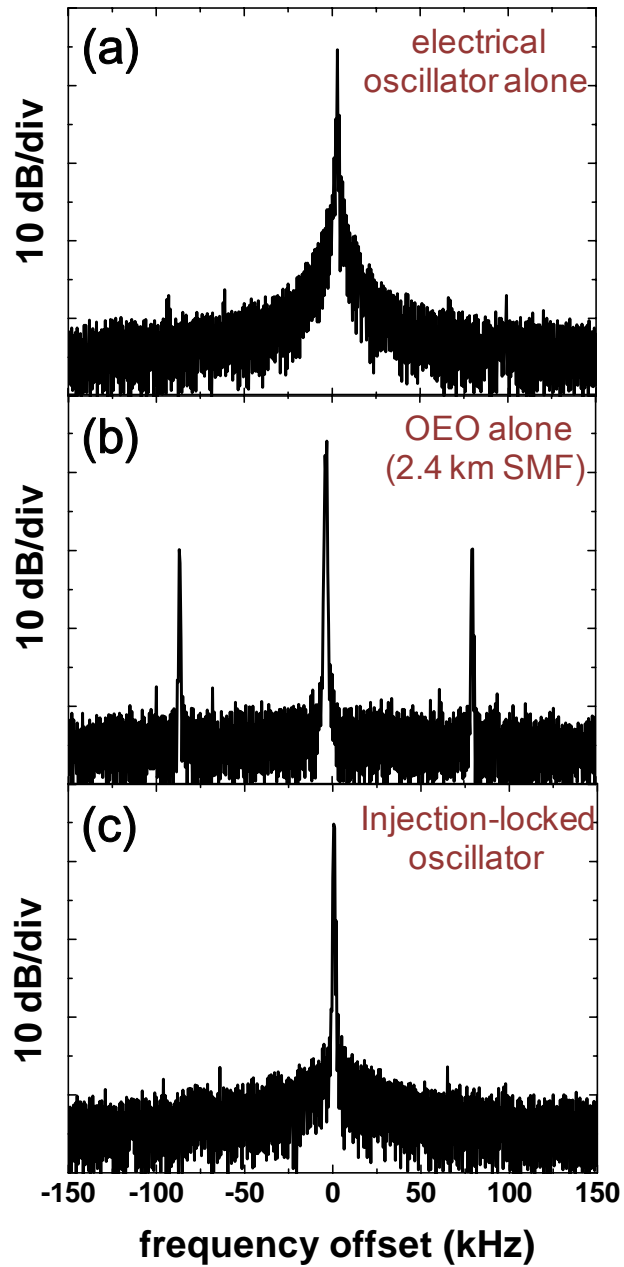


Fig.3-4. Measured output spectra of (a) electrical oscillator, (b) OEO having 2.4-km long SMF, and (c) injection-locked oscillator. The center frequencies are 30.0092985 GHz, 30.0071960 GHz, and 30.0092985 GHz, respectively.

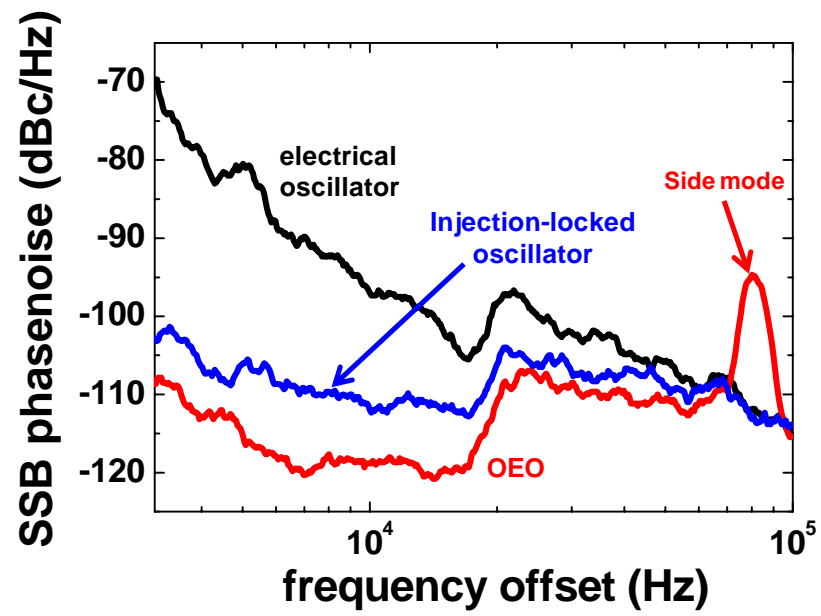


Fig.3-5. Measured phase noises of output signals from the electrical and injection-locked oscillator, and OEO.

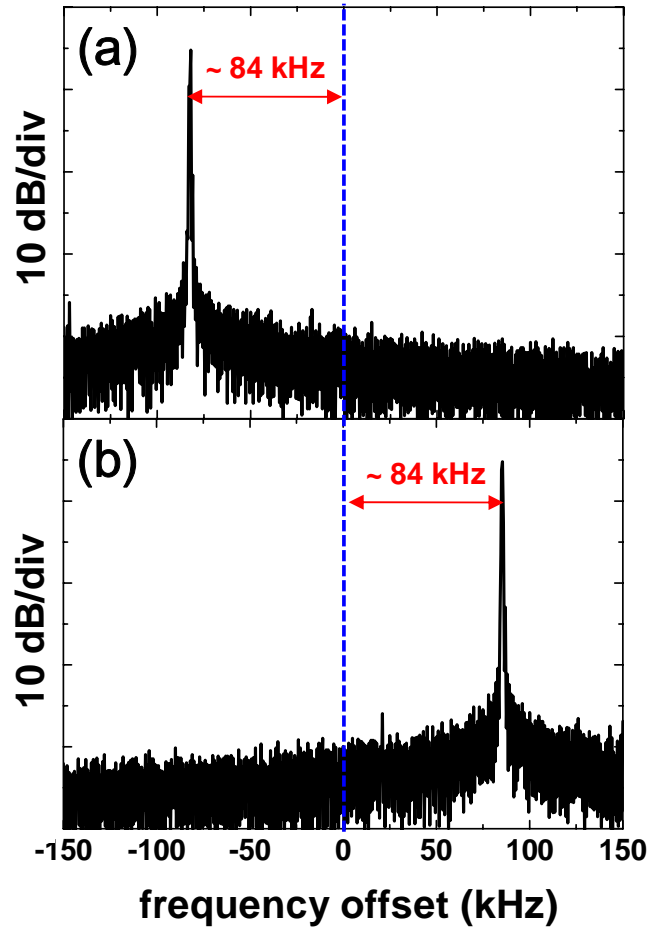


Fig.3-6. Measured spectra of different OEO modes selected by tuning the phase shifter.

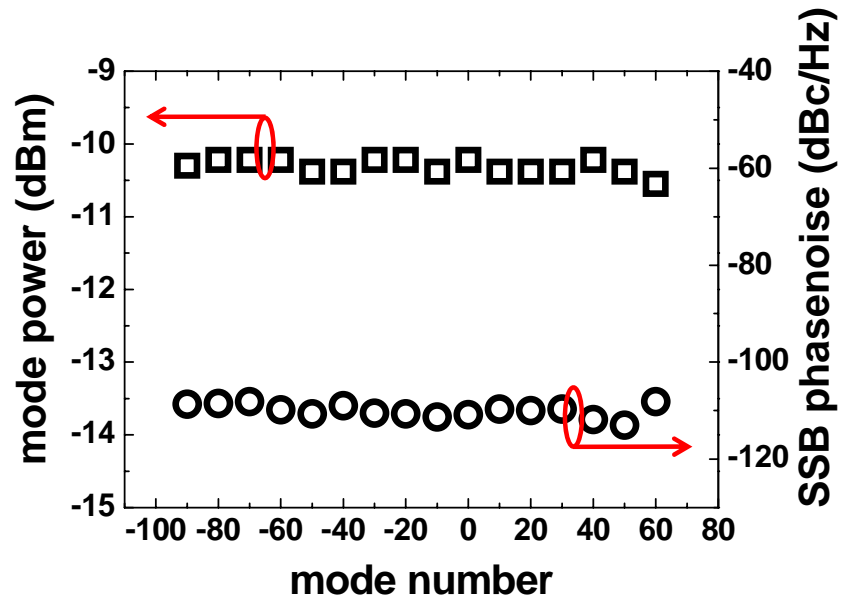


Fig.3-7. SSB phase noise values measured at 10-kHz frequency offset and the mode power for the selected modes.

### **3-4. Conclusion**

A simple and cost-effective technique for single-mode oscillation in an OEO was proposed. The proposed scheme extracted a desired mode from multiple modes in an OEO at 30-GHz bands by injecting OEO modes into an electrical oscillator. Although the phase noise is degraded about 6 dB at 10-kHz frequency offset by injection-locking, extraction of a desired OEO mode among many OEO modes separated by about 84 kHz at 30-GHz bands can be successfully achieved.

However, the proposed scheme could not produce the optical signal modulated by the generated high spectral-purity electrical signal since an electrical oscillator was used as a slave oscillator.

In order to solve this problem, a new hybrid oscillator will be proposed by using self-injection locking in the next chapter.

## **Chapter 4**

# **Optoelectronic Self-Injection-Locked Oscillator**

### **4-1. Introduction**

This chapter will propose an optoelectronic self-injection-locked (SIL) oscillator with a long optical delay line that can significantly reduce the output phase noise. Unlike the previous injection-locked OEO, it can generate intensity modulated optical signals as well as a high spectral-purity millimeter-wave signal.

The proposed oscillator uses a self-injection-locking method for the output phase-noise reduction. Thus, we will begin with the general phase-noise characteristic of a typical RF SIL oscillator and then present the new optoelectronic SIL oscillator.

## 4-2. Conventional SIL oscillator

A self-injection-locked (SIL) oscillator has been actively investigated for generation of stable and low phase-noise signals [18-21]. It can be easily realized by self-injection of a part of output signals after passing through a high quality-factor (Q) external resonator or a long delay line, as shown in Fig. 4-1.

In this section, the RF SIL oscillator's phase-noise characteristic will be briefly discussed.

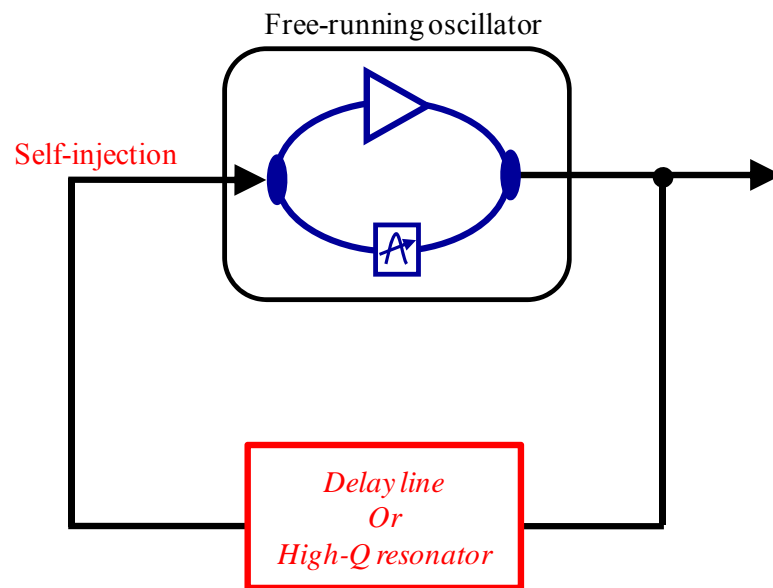


Fig.4-1. Self-injection-locked oscillator.

#### 4-2-1. Phase noise of SIL oscillators

The phase dynamics of the SIL oscillator depends on the coupling signal's phase and power, and the types of the oscillator circuits. If the transfer function and time domain response of the feedback circuit are set by  $H(\omega)$  and  $h(t)$ , respectively, the phase relationship of the SIL oscillator can be expressed by [19]

$$\frac{d\theta(t)}{dt} = \omega_0 + \rho\omega_{3dB} \sin(\theta_{inj}(t) - \theta(t)) - \omega_{3dB}N(t) \quad (4.1)$$

where  $\omega_0$  is the oscillation frequency,  $\theta(t)$ ,  $\theta_{inj}(t) = h(t) * \theta(t)$  are the instantaneous phases of the oscillator output signal and the injection signal, respectively,  $\omega_{3dB}$  is the half-width at half maximum of the oscillator tank circuit,  $\rho$  is the injection signal's amplitude normalized by oscillator output amplitude, and  $N(t)$  is time-varying noises.

If we assume the noise is small perturbation to a noise free solution, we can write

$$\theta(t) \rightarrow \hat{\theta}(t) + \delta\theta(t) = \omega_0 t + \delta\theta(t) \quad (4.2)$$

$$\theta_{inj}(t) \rightarrow \hat{\theta}_{inj}(t) + \delta\theta_{inj}(t) \quad (4.3)$$

$$e^{j\delta\theta(t)} \approx 1 + j\delta\theta(t). \quad (4.4)$$

Therefore, the phasor expression of the injected signal is

$$\begin{aligned} F[e^{j\delta\theta_{inj}(t)}] &= F[e^{j(\tilde{\theta}_{inj}(t) + \delta\theta_{inj}(t))}] \\ &\approx F[e^{j\tilde{\theta}_{inj}(t)}] + jF[e^{j\tilde{\theta}_{inj}(t)}\delta\theta_{inj}(t)] \\ &= H(\omega)F[e^{j\theta(t)}] \\ &= H(\omega)F[e^{j(\omega_0 t + \delta\theta(t))}] \\ &\approx H(\omega)(F[e^{j\omega_0 t}] + jF[e^{j\omega_0 t}\delta\theta(t)]) \\ &= H(\omega)\delta(\omega - \omega_0) + jH(\omega)\delta\tilde{\theta}(\omega - \omega_0) \end{aligned} \quad (4.5)$$

where  $\delta(\omega)$  is the Dirac delta function.

From (4.5), the phase fluctuation of the injection signal around the oscillation frequency in the frequency domain is

$$F[e^{j\tilde{\theta}_{inj}(t)}\delta\theta_{inj}(t)] = \delta\tilde{\theta}_{inj}(\omega - \omega_0) = H(\omega)\delta\tilde{\theta}(\omega - \omega_0) \quad (4.6)$$

and the relationship in the time domain is

$$\delta\theta_{inj}(t) = (h(t)e^{-j\omega_0 t}) * \delta\theta(t). \quad (4.7)$$

From (4.7) and (4.1), the phase fluctuation can be obtained by

$$\frac{d\delta\theta(t)}{dt} = +\rho\omega_{3dB} \cos(\Delta\hat{\theta}_p) [(h(t)e^{-j\omega_0 t}) * \delta\theta(t) - \delta\theta(t)] - \omega_{3dB}N(t). \quad (4.8)$$

where  $\Delta\hat{\theta}_p = \hat{\theta}(t) - \hat{\theta}(t-T)$ .

Fourier transforming (4.8) gives

$$\delta\tilde{\theta}(\omega) = \frac{-\omega_{3dB}\tilde{N}(\omega)}{j\omega - \rho\omega_{3dB} \cos(\Delta\hat{\theta}_p)[H(\omega_0 + \omega) - 1]} \quad (4.9)$$

where  $\omega$  is the offset frequency from the oscillation frequency  $\omega_0$ .

The phase noise power spectrum ( $\langle \delta\tilde{\theta}(\omega)\delta\tilde{\theta}^*(\omega) \rangle$ ) of a SIL oscillator can be obtained from (4.9) with a feedback transfer function  $H(\omega)$ :

$$|\delta\tilde{\theta}(\omega)|^2 = \frac{|\delta\tilde{\theta}_0(\omega)|^2}{\left| j + \rho\left(\frac{\omega_{3dB}}{\omega}\right)\cos(\Delta\hat{\theta}_p) - \rho\left(\frac{\omega_{3dB}}{\omega}\right)H(\omega_0 + \omega) \right|^2}. \quad (4.10)$$

**4-2-2. Phase noise of the SIL oscillator having a long delay-line in the feedback route**

The transfer function of a delay-line feedback loop is

$$H(\omega) = e^{-j\omega T} \quad (4.11)$$

where  $T$  is the loop delay time [19]. In (4.11), it is assumed that the delay-line loss is very small and negligible.

From (4.10) and (4.11), the phase fluctuation of a SIL oscillator having a delay line as a feedback loop is

$$\begin{aligned} \frac{|\delta\tilde{\theta}(\omega)|^2}{|\delta\tilde{\theta}_0(\omega)|^2} &= [1 + 2\rho\omega_{3dB} \cos(\omega_0 T) \left(\frac{\sin(\omega_0 + \omega)T}{\omega}\right) \\ &\quad + 2(\rho\omega_{3dB} \cos(\omega_0 T))^2 \left(\frac{1 - \cos(\omega_0 + \omega)T}{\omega^2}\right)]^{-1} \end{aligned} \quad (4.12)$$

If the loop phase  $\Delta\hat{\theta}_p = \omega_0 T = 2m\pi$  (m: integer), (4.12) becomes

$$\frac{|\delta\tilde{\theta}(\omega)|^2}{|\delta\tilde{\theta}_0(\omega)|^2} = \frac{1}{1 + 2\rho\omega_{3dB}\left(\frac{\sin \omega T}{\omega}\right) + 2(\rho\omega_{3dB})^2\left(\frac{1 - \cos \omega T}{\omega^2}\right)}. \quad (4.13)$$

From (4.13), the phase noise near the oscillation frequency can be expressed by

$$\lim_{\omega \rightarrow 0} |\delta\tilde{\theta}(\omega)|^2 \rightarrow \frac{|\delta\tilde{\theta}_0(\omega)|^2}{(1 + \rho\omega_{3dB}T)^2}. \quad (4.14)$$

As the self-injection power and the loop delay increases, the lower phase noise can be obtained near the oscillation frequency offset.

**4-2-3. Phase noise of the SIL oscillator having a high- $Q$  resonator in the feedback route**

Instead of a delay-line cable, a high- $Q$  resonator can stabilize the oscillator signals and reduce output phase noise in the feedback loop [19].

The transfer function of the high- $Q$  resonator can be written as

$$H(\omega) = \frac{j\omega \frac{\omega_r}{Q_r}}{(\omega_r^2 - \omega^2) + j\omega \frac{\omega_r}{Q_r}} \quad (4.15)$$

where  $\omega_r$  and  $Q_r$  are the resonance frequency and  $Q$  factor of the resonator, respectively.

For the sake of simplicity, we assume that the resonance frequency of the resonator is same with the oscillation frequency and the phase noise of the self-injection-locked oscillator becomes

$$\frac{|\delta\tilde{\theta}(\omega)|^2}{|\delta\tilde{\theta}_0(\omega)|^2} = \frac{1 + \left(\frac{\omega}{\omega_{3dB}}\right)^2 \left(\frac{Q_r}{Q}\right)^2}{\left(1 + \rho \frac{Q_r}{Q}\right)^2 + \left(\frac{\omega}{\omega_{3dB}}\right)^2 \left(\frac{Q_r}{Q}\right)^2}. \quad (4.16)$$

In the equation, it is assumed that  $\Delta\hat{\theta}_p = \omega_0 T = 2m\pi$ .

For the phase noise near the oscillation frequency

$$\lim_{\omega \rightarrow 0} |\delta\tilde{\theta}(\omega)|^2 \rightarrow \frac{|\delta\tilde{\theta}_0(\omega)|^2}{(1 + \rho \frac{Q_r}{Q})^2}. \quad (4.17)$$

From (4.17), it can be known that the phase noise reduction is determined by the  $Q$  factor ratio of the high- $Q$  resonator in the feedback loop to the oscillator. It is because that the high- $Q$  resonator operates as a band pass filter which shapes the spectrum of the self-injection signal.

### **4-3. Proposed SIL oscillator**

#### ***4-3-1. Motivation***

With the self-injection-locking method, many successful demonstrations have been reported in RF domain [18-21]. For example, phase noises of about -50 dBc/Hz (20-dB phase-noise reduction) at 10-kHz offset for 8-GHz band [18] and -120.1 dBc/Hz (4-dB phase-noise reduction) at 1-MHz offset for 9.6-GHz band [20] have been achieved by a delay line in the feedback loop, while -95 dBc/Hz at 100-kHz offset for 60-GHz band has been obtained by a ceramic high-Q resonator in the feedback loop [21].

Although it is possible to further reduce phase noises in RF domain by using a longer delay line or a higher Q external resonator, they are very impractical especially for millimeter-wave applications, since the delay line length is limited by large loss and high-Q devices are not easily available.

On the other hand, long optical delay lines have been used for generation of a very high-Q external resonator in an optoelectronic oscillator (OEO) due to low transmission loss of optical fiber [5-11]. An OEO can generate high-spectral-purity micro-/millimeter waves

with a long optical delay line, but the optical loop should have loop gain for self-oscillation, requiring very high electrical and optical gain to compensate the large electrical-to-optical-to-electrical (E/O/E) conversion loss.

To solve above problems, a new SIL oscillator having a long optical delay line as a passive feedback route is proposed.

### ***4-3-2. Proposed scheme and operation principle***

The proposed optoelectronic SIL oscillator has a similar structure to a typical dual-loop OEO, but it is simpler and more cost-effective, as can be seen in Fig. 4-2. The shorter optical loop in the dual-loop OEO is replaced by an electrical loop composed of an electrical amplifier and an RF filter and the longer optical loop is used for self-injection of the output signal from the electrical loop.

The electrical loop has sufficient gain to oscillate by itself, while the optical loop does not. Therefore, the optical loop works as a feedback route for self-injection of an electrical-loop output signal.

A part of output signals from the electrical oscillator, as can be seen in Fig. 4-2 (b), is injected into the oscillator after passing through a long optical delay line and it locks the electrical oscillator, achieving self-injection locking. Once the oscillator is locked by the delayed replica of its output signal, its frequency and phase fluctuations are reduced and the phase-noise reduction ratio ( $\eta$ ) near the carrier frequency can be described as [22]

$$\lim_{\omega \rightarrow 0} \eta(\omega) \rightarrow \frac{1}{(1 + \sqrt{\kappa} \omega_{3dB} \tau)^2}, \quad (4.18)$$

where  $\omega$  is the offset frequency from the center frequency,  $\tau$  is the optical-loop delay,  $\omega_{3dB}$  is the half-width-at-half-maximum of the resonator inserted in the electrical oscillator, and  $\kappa$  is the self-injection power normalized to the oscillator output power. In (4.18), it is assumed that there is no steady-state phase difference between self-injected and oscillator output signals. As shown in Eq. (4.18), a longer delay line or larger power injection produces more phase noise reduction. In this demonstration, 2.4-km long single-mode fiber (SMF) was used as a delay line.

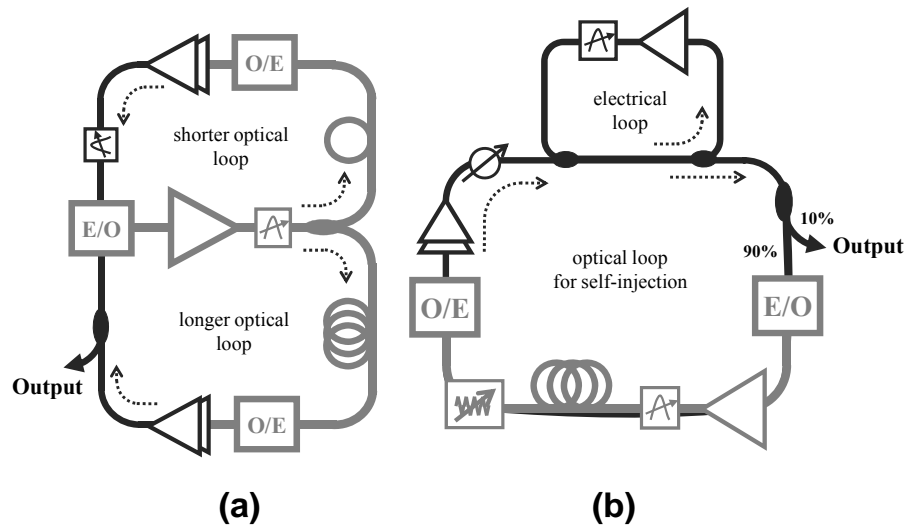


Fig.4-2. Configurations of (a) a typical dual-loop OEO and (b) the proposed self-injection-locked oscillator having a long optical delay line.

### ***4-3-3. Experimental setup and results***

As shown in Fig. 4-3, the electrical loop was configured with an electrical amplifier having RF gain of about 18 dB, an RF filter having  $Q$  of 1000 at 30 GHz with about 3.16-dB insertion loss, and a 4-port 3-dB RF coupler having insertion loss of about 1.8 dB. 90 % of output signals from the electrical loop were converted to optical signals by an E/O converter made up of a tunable laser source and a Mach-Zehnder Modulator (MZM) having 40-GHz modulation bandwidth, and passed through 2.4-km long SMF.

These optical signals were converted again to electrical signals by a high-speed photo diode having 60-GHz bandwidth and self-injected to lock the electrical oscillator. An Er-doped fiber amplifier and two electrical amplifiers having the total gain of about 46 dB were inserted to partially compensate large conversion (E/O/E) loss, and an optical filter was inserted for filtering out the lower sideband in MZM output signals to avoid any RF signal-fading problem induced by fiber dispersion [23]. The power and phase of self-injected signals were adjusted by an optical attenuator and an RF phase shifter, respectively.

10% of output signals from the electrical loop were measured by an RF spectrum analyzer (HP8563E) connected with an external mixer (HP11970A) having conversion loss of about 26 dB after attenuation of

about 2.67 dB. This attenuation was needed due to the display limit (-6.1 dBm) of the spectrum analyzer used in the measurement.

The output spectra measured at various  $\kappa$  are shown in Fig. 4-4. Fig. 4-4 (a) is the output spectrum measured at  $\kappa=0$  (no self-injection), while (b) and (c) are the spectra measured at  $\kappa$  of  $1.6\times 10^{-3}$  and  $2.5\times 10^{-1}$ , respectively. These figures show that self-injection-locking reduces phase noise and larger  $\kappa$  provides larger improvement. However, unwanted side modes separated by about 84 kHz from the center frequency can be observed in Fig. 4-4 (b) and (c), and they increase as  $\kappa$  increases. These are due to coupled-loop oscillation. Although the optical loop cannot oscillate alone due to large loop loss, the coupled-loop can oscillate if electrical-loop gain compensates optical-loop loss [9]. Therefore, as the injection power increases, causing optical-loop loss reduction, the coupled-modes become stronger. These unwanted signals can be suppressed by adding an additional optical delay line having different length [11].

In order to clearly verify the phase-noise-reduction performance, single-sideband (SSB) phase noises of output signals shown in Fig. 4-4 were measured and the results are shown in Fig. 4-5. The measured phase-noise values at 10-kHz frequency offset are -91.83 dBc/Hz ( $\kappa=0$ ), -110.17 dBc/Hz ( $\kappa=1.6\times 10^{-3}$ ), and -118.5 dBc/Hz ( $\kappa=2.5\times 10^{-1}$ ). The

phase-noise peaking at  $\sim 20$ -kHz frequency offset is believed due to our measurement setup using an external mixer. Clearly, the self-injection locking drastically enhances phase quality of output signals.

Fig. 4-6 shows dependency of SSB phase noises measured at 10-kHz frequency offset and SMSR on  $\kappa$ . As shown in the figure, both SMSR and SSB phase noises are reduced with increasing  $\kappa$ . For  $\kappa$  larger than  $10^{-2}$ , phase noises are saturated due to the sensitivity limit of our spectrum analyzer used in the measurement.

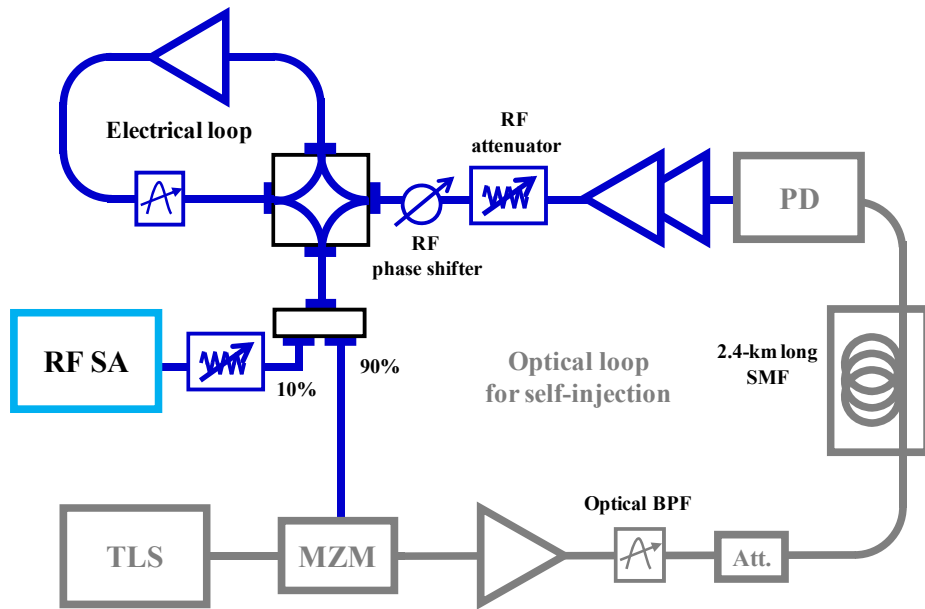


Fig.4-3. Experimental setup for demonstration of optoelectronic self-injection-locked oscillator.

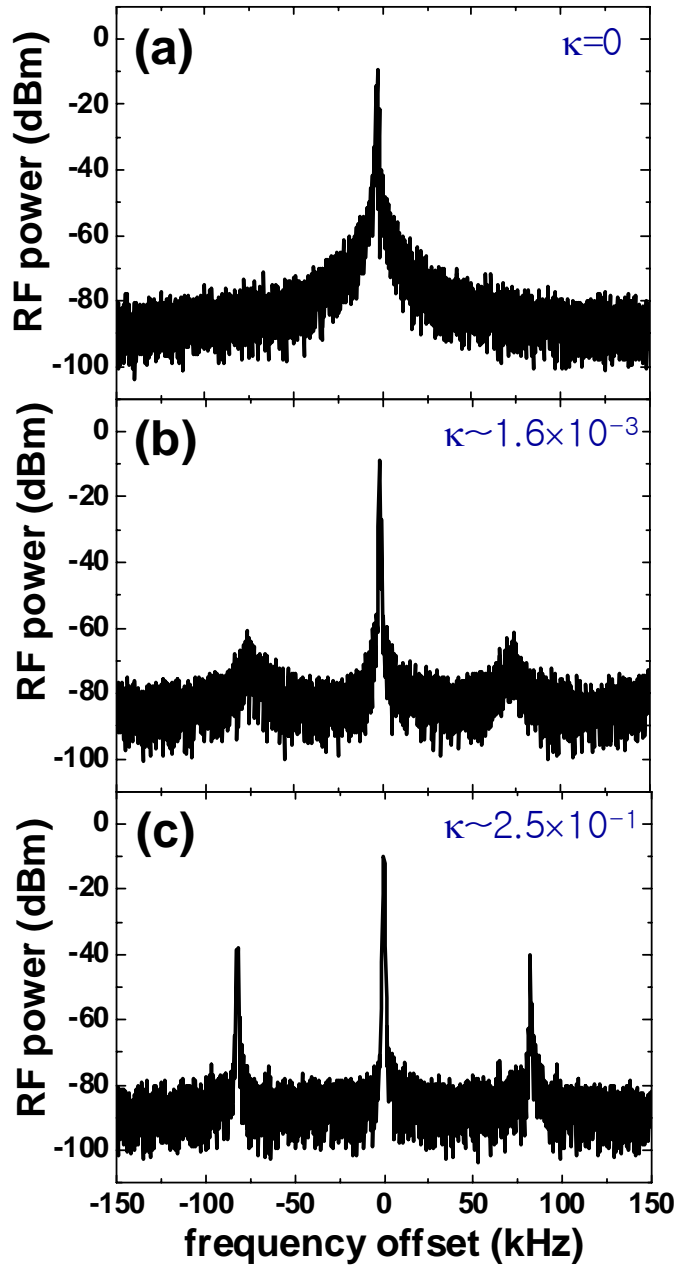


Fig.4-4. Measured RF spectra of the output signals at (a)  $\kappa=0$ , (b)  $\kappa\sim 1.6\times 10^{-3}$ , and (c)  $\kappa\sim 2.5\times 10^{-1}$ . The center frequencies are 29.9773362 GHz, 29.9770507 GHz, and 29.9768307 GHz, respectively. In all figures, the frequency span and resolution bandwidth settings were 300 kHz and 300 Hz, respectively.

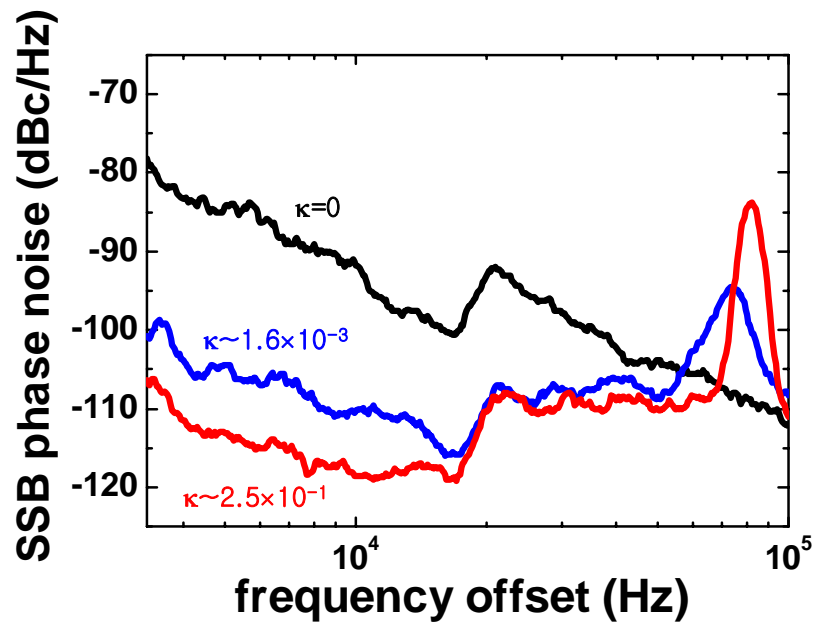


Fig.4-5. Measured phase noises of the output signals at (a)  $\kappa=0$ , (b)  $\kappa\sim 1.6\times 10^{-3}$ , and (c)  $\kappa\sim 2.5\times 10^{-1}$ .

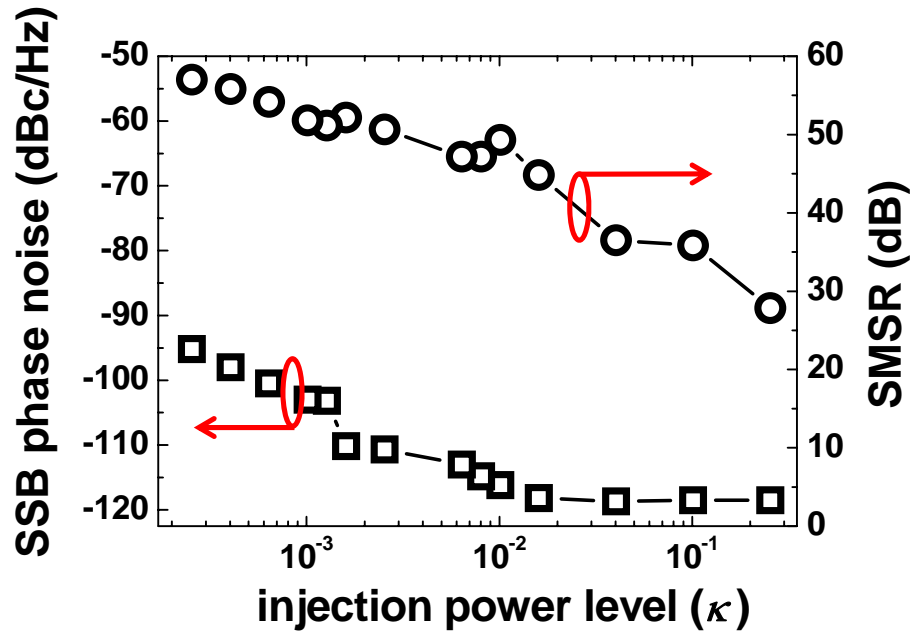


Fig.4-6. SSB phase noises at 10-kHz frequency offset from the center frequency and SMSR according to the injection power level.

### *4-3-3.Summary*

Optoelectronic SIL oscillators with 2.4-km long SMF as an optical long feedback line for output phase-noise reduction have been demonstrated at 30-GHz bands and it has been found that the higher self-injection power provides larger phase-noise reduction but with lower SMSR. At the injection-power level of about  $1.6 \times 10^{-3}$ , 30-GHz oscillation with SMSR larger than 50 dB and the output phase-noise reduction of about 18 dB at 10-kHz frequency offset have been successfully demonstrated.

## **4-4. Compact and low-cost configuration for an optoelectronic SIL oscillator**

### ***4-4-1.Motivation***

The previously proposed optoelectronic SIL oscillator can produce low-phase noise signal with high SMSR by controlling the self-injection power. In addition, it can generate optical signals modulated by the resulting low-phase noise RF signals, which are useful for various photonic applications.

However, it requires high-speed optical components for electrical-to-optical (E/O) and optical-to-electrical (O/E) conversions. Generally, the conversion efficiency of the practical high-speed optical components is very low and expensive, resulting in high cost for realization of the optoelectronic SIL oscillator.

In the following sections, a compact and low cost configuration for an optoelectronic SIL oscillator will be proposed and demonstrated.

#### ***4-4-2. Proposed configuration for an optoelectronic SIL oscillator***

Basically, an optoelectronic SIL oscillator consists of an electrical free-running oscillator and a long optical feedback loop. For the compact and low-cost configuration, the free-running oscillator is realized with an InP monolithic heterojunction photo-transistor (HPT) oscillator which also performs optical-to-electrical (O/E) conversion. Electrical-to-optical (E/O) conversion is performed with two low-speed and low-cost laser diodes (LDs).

Fig. 4-7 shows the proposed configuration. The E/O conversion scheme is essentially same as the technique which is previously reported for overcoming LD modulation bandwidth limitation [24]. As shown in the figure, no high-speed and high-cost optical/optoelectronic components are used in the configuration.

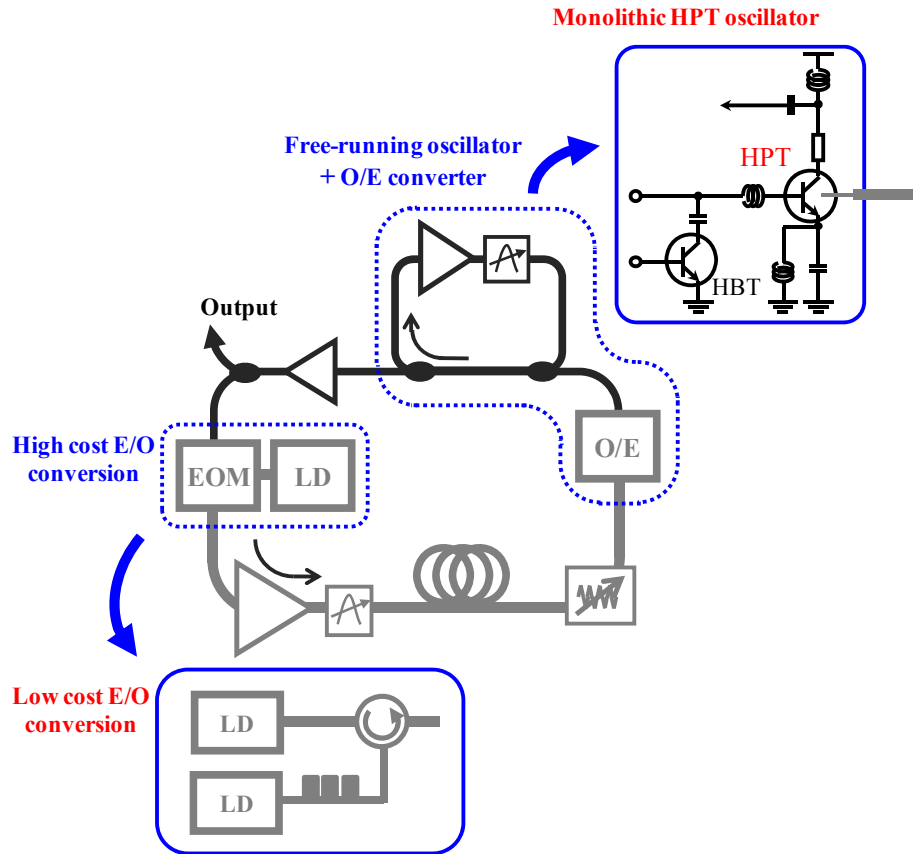


Fig.4-7. Compact and low cost configuration for an optoelectronic SIL oscillator based on a monolithic HPT oscillator and low cost optical components.

### ***4-4-3. Operation principle***

The proposed scheme can be divided into three parts: an E/O converter, a monolithic free-running oscillator performing O/E conversion as well, and a total loop including a long delay line.

Fig. 4-8 shows the E/O converter made up of two LDs and schematic optical spectra. One of LDs is directly modulated by injected RF signals, producing two side bands in the wavelength domain as shown in the figure. These side bands are very weak since LD1 is not fast enough for injected RF signals. Once these optical modes are injected into LD2 through an optical circulator, only the optical modes within the gain wavelength range of LD2 obtain optical gain.

The gain wavelength range marked by the shade region in Fig. 4-8 is determined by LD2 lasing wavelength and the injected optical power [24, 25]. Moreover, the gain curve is asymmetric. The optical mode at the longer wavelength receives larger gain than the one at the lower wavelength, which is quite useful for enhancing the weak sideband. The asymmetric gain curve can be generally explained as follows. If the slave LD (LD2) is injected by the external optical signal, the carrier density in the active region decreases. The decreased carrier density leads to increase in the refractive index of the active region, resulting in

the lowering of the cavity resonance frequency. Namely, the injected optical sideband at the shorter frequency (longer wavelength) can obtain the cavity gain [25].

By controlling the temperature or the bias current for LD2, only the desired side mode can be amplified and this results in enhancement of the modulation depth as well as the single sideband optical spectrum which can avoid RF signal-fading problem induced by fiber dispersion [23].

The output signals from the E/O converter are injected into the HPT based monolithic oscillator after passing through a long optical delay line. The  $\text{In}_{0.53}\text{Ga}_{0.47}\text{As}$  layer of the HPT can detect 1.55- $\mu\text{m}$  optical signals and the photo-detected RF signals lock the HPT free-running oscillator, achieving self-injection locking.

Once the oscillator is self-locked by the delayed replica of its output signal, its frequency and phase fluctuations are reduced. The phase-noise reduction ratio ( $\eta$ ) near the carrier frequency can be described as

$$\lim_{\omega \rightarrow 0} \eta(\omega) \rightarrow \frac{1}{(1 + P_{opt} \cdot \tau \cdot M)^2} \quad (4.19)$$

where  $\omega$  is the offset frequency from the center frequency,  $P_{opt}$  is the

injected optical power to the HPT,  $\tau$  is the optical-loop delay.  $M$  is the characteristic parameter of the HPT oscillator given as

$$M = \omega_{3dB} \sqrt{\frac{\rho^2 R}{P_{out}}} \quad (4.20)$$

where  $\omega_{3dB}$  is the half-width-at-half-maximum of the resonator in the HPT oscillator,  $\rho$  is the photo-responsivity and  $R$  is the load impedance of the HPT and  $P_{out}$  is the oscillator output power. As expected, a longer delay line or larger optical power injection produces more phase noise reduction.

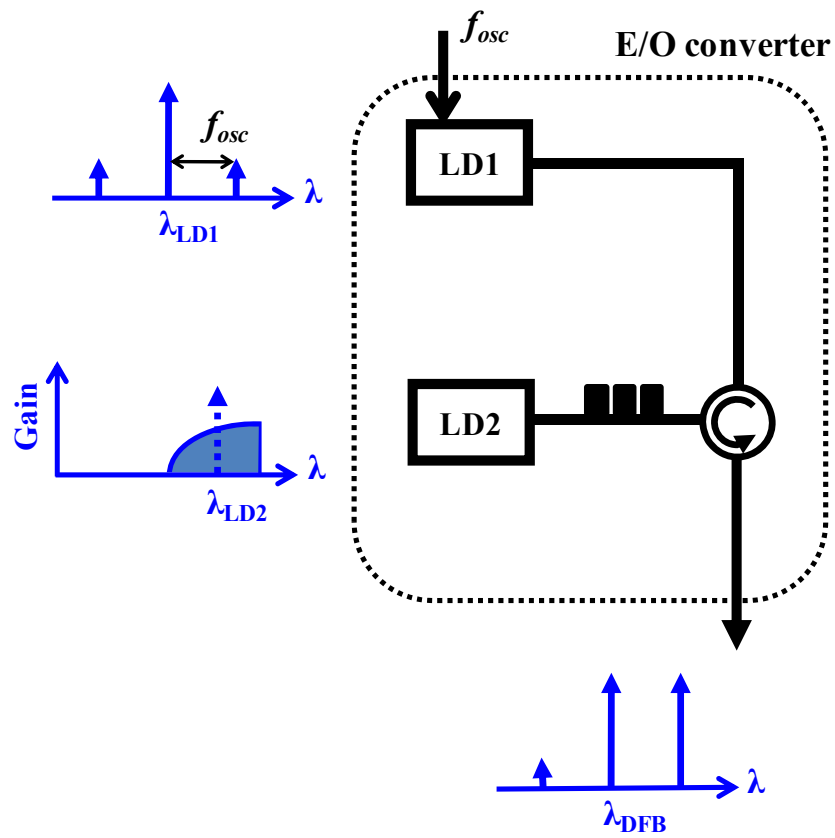


Fig.4-8. E/O converter and schematic optical spectra. The shade region means the gain wavelength range of LD2 and  $\lambda_{LD2}$  is the wavelength of LD2 without any optical injection.

#### ***4-4-4. Experimental setup and results***

Fig. 4-9 shows the experimental setup for demonstration of the new configuration for the optoelectronic SIL oscillator. The HPT based monolithic oscillator used in this demonstration has the optical window with 5- $\mu$ m diameter on the top of the emitter for photo-detection and the chip size is only  $0.7 \times 0.54$  mm [26]. The detailed description of the HPT oscillator is shown in Fig. 4-10. The electrical current gain cutoff frequency is 153 GHz and the photo-transistor internal gain is about 18 dB at 10-GHz optical modulation frequency [26]. The free-running frequency and quality factor of the oscillator can be controlled by adjusting the bias voltage for the HBT inserted in the oscillator. In this investigation, the bias was set for 10.8 GHz oscillation.

The E/O converter was configured with two LDs, one of which is a commercial 2.5-Gb/s distributed-feedback (DFB) LD (LD1) and the other is a commercial Fabry-Pérot (FP) LD (LD2) without an isolator. The modulation efficiency of the DFB LD at 10 GHz was about 15 dB lower than at 1 GHz. The FP LD was used since it has many optical modes providing easier selection of the desired mode for the wavelength-selective amplification process.

50 % of the output signals from the HPT oscillator directly

modulated the DFB laser and the modulated optical signal was injected into the FP-LD. With the external optical injection, all undesired lasing modes of the FP-LD were greatly suppressed. By controlling the temperature of the FP-LD, the gain region was moved to the side mode located at the longer wavelength from the optical carrier.

The optical spectra measured before and after the FP-LD are shown in Fig. 4-11 (a) and (b), respectively. Although the resolution bandwidth (0.07 nm) of the used optical spectrum analyzer (OSA) was not high enough to distinguish each mode, Fig. 4-11 (b) clearly shows that the side mode located at the longer wavelength was amplified by the FP-LD.

The output signals from the E/O converter passed through a 2.4-km long single mode fiber and they were injected into the HPT oscillator. The HPT photo-detected the optical signals at Tr-mode to obtain high internal gain of about 20 dB at 10 GHz. An Er-doped fiber amplifier (EDFA) and an electrical amplifier having 30-dB gain were inserted to partially compensate the large conversion (E/O/E) loss, and an optical filter was inserted for filtering out the EDFA amplified spontaneous emission (ASE) noise.

50% of the output signals from the optoelectronic SIL oscillator was measured by an RF spectrum analyzer (HP8563E) and Fig. 4-12 shows

the output spectra measured at different optical power values injected into the HPT oscillator. Fig. 4-12 (a) shows the output spectrum of the free-running HPT oscillator (no optical signal injection), while (b) and (c) are the spectra measured at the injection optical power of -6 dBm and 8 dBm, respectively. These figures show that self-injection-locking enhances the signal quality and larger injection optical power provides larger improvement. However, unwanted side modes separated by about 84 kHz from the center frequency can be observed in Fig. 4-12 (b) and (c). As mentioned in the previous section, these are due to coupled-loop oscillation and they can be suppressed by adding an additional optical delay line having different length [11].

Fig. 4-13 shows the dependency of single sideband (SSB) phase noises measured at 10-kHz frequency offset on the optical injection power. As shown in the figure, SSB phase noises reduce with increasing the injection power and the reduction level (20 dB/decade) agrees well with the Eq. (4-19).

Fig. 4-14 shows the single-sideband (SSB) phase noises of the output signals shown in Fig. 4-13. The measured phase-noise values at 10-kHz frequency offset are -44.17 dBc/Hz (free-running), -76.83 dBc/Hz ( $P_{opt} = -6$  dBm), and -100.00 dBc/Hz ( $P_{opt} = 8$ dBm). Clearly, the self-injection locking drastically enhances the phase quality of the output

signal and about 55-dB phase-noise reduction can be achieved by 8-dBm optical injection.

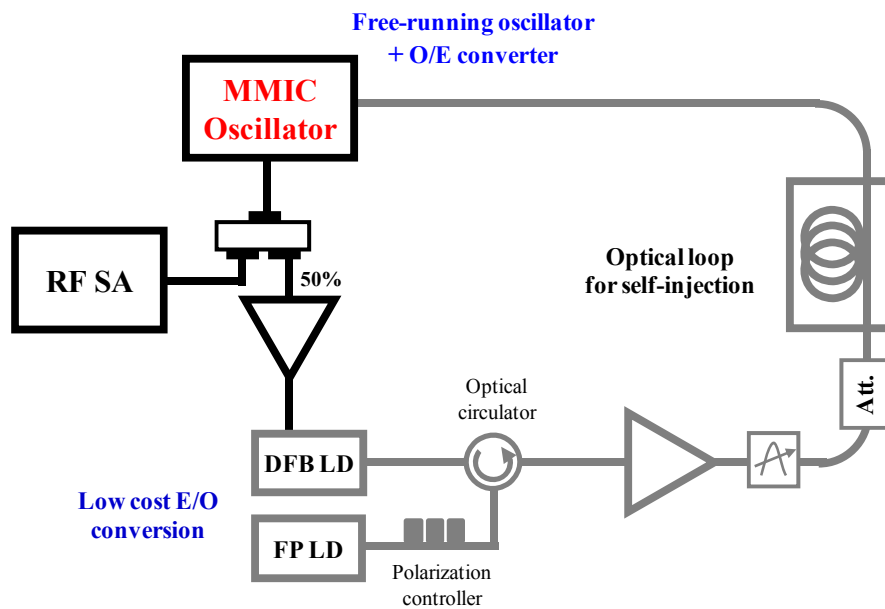


Fig.4-9. Experimental setup for demonstration of a new configuration for an optoelectronic SIL oscillator.

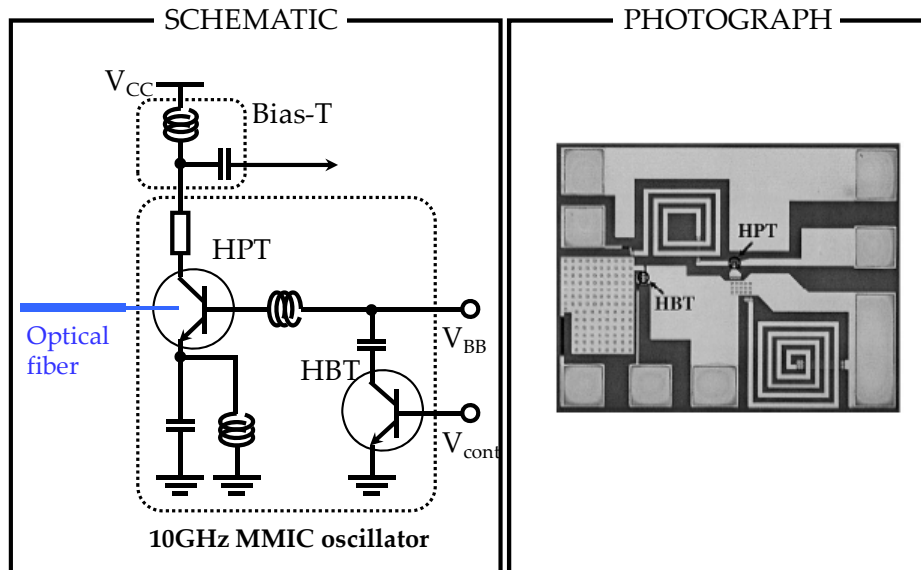


Fig.4-10. Schematic and photograph (from [26]) of HPT based monolithic oscillator.

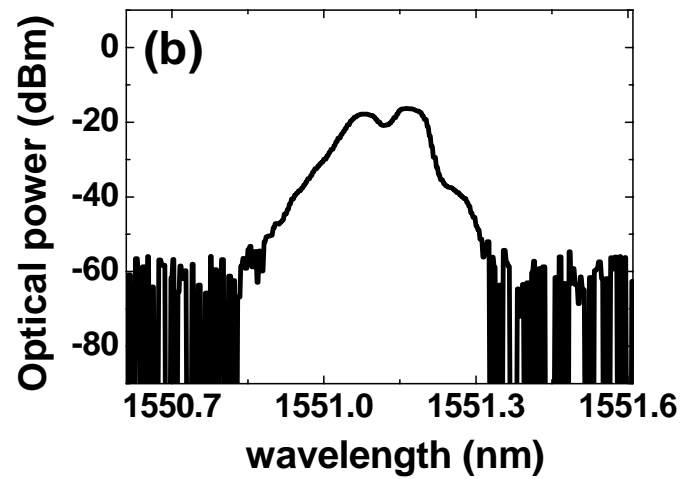
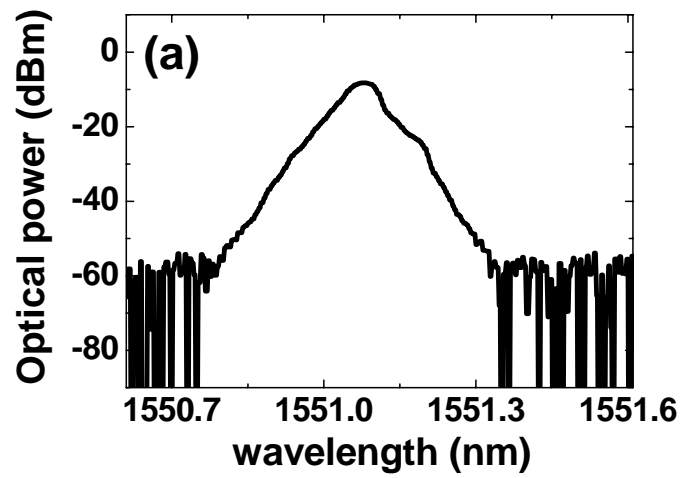


Fig.4-11. Measured optical spectra of the output signals from (a) the DFB LD directly modulated by the HPT-oscillator-output signal and (b) the FP LD with optical injection of the modulated output signals.

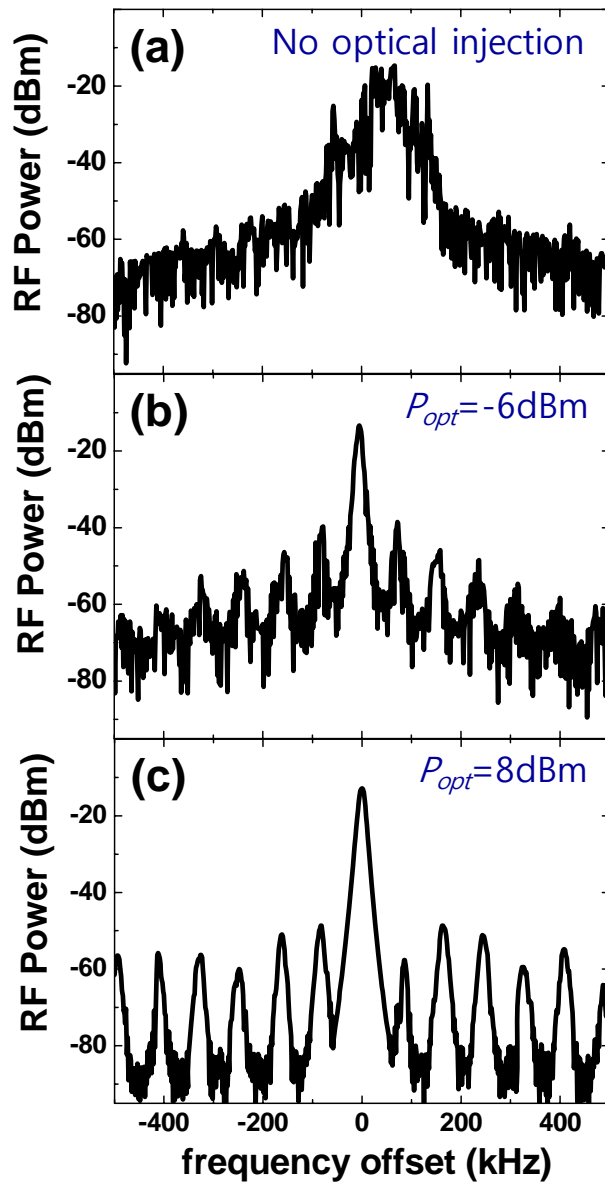


Fig.4-12. Measured RF spectra of the output signals for (a) no optical signal injection, (b)  $P_{opt} = -6$  dBm, (c)  $P_{opt} = 8$  dBm. The center frequencies are 10.790847 GHz, 10.790693 GHz and 10.790314 GHz, respectively. In all figures, the frequency span and resolution bandwidth settings were 1 MHz and 10 kHz, respectively.

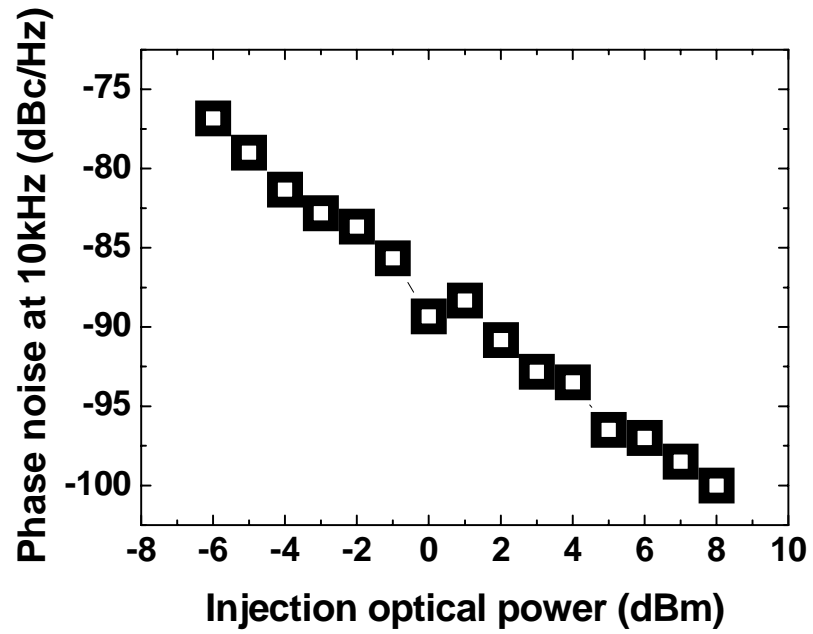


Fig.4-13. SSB phase noises at 10-kHz frequency offset from the center frequency according to the injection optical power level.

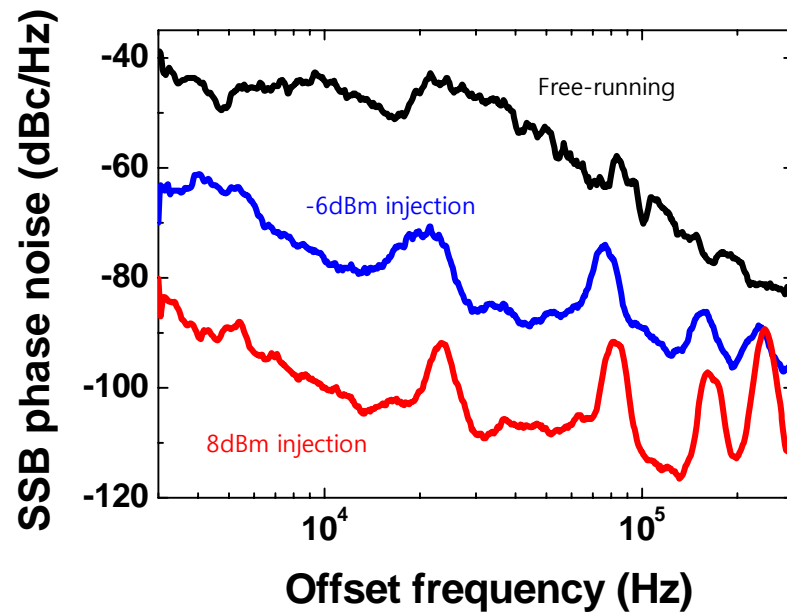


Fig.4-14. Measured phase noises of the optoelectronic output signals at different injection optical power values.

#### *4-4-5.Summary*

In this section, a compact and low cost optoelectronic SIL oscillator has been proposed and demonstrated. The proposed scheme does not require any high-speed optical and optoelectronic components since E/O and O/E conversion are performed by a HPT based monolithic oscillator operating as a free-running oscillator as well and two low-speed LDs, respectively. With this proposed scheme, about 55-dB phase-noise reduction at 10-kHz frequency offset from the center frequency of about 10.8 GHz has been successfully demonstrated.

## 4-5. Conclusion

In this chapter, optoelectronic SIL oscillators, where a part of the electrical output signal is self-injected after passing through a long optical feedback loop for output phase-noise reduction, has been demonstrated.

First of all, the optoelectronic SIL oscillator has been realized with an electrical oscillator composed of commercially available modules such as an RF amplifier and an RF BPF, and a long optical feedback loop. This optoelectronic SIL oscillator can overcome the limited  $Q$  of the electrical resonator by using a long optical delay line. However, high-speed optical and optoelectronic components for electrical-to-optical (E/O) and optical-to-electrical (O/E) conversions are required for its realization. Moreover, commercially available high-speed optical components have low conversion efficiency and they are very expensive.

In order to overcome the problems, a new configuration, which uses an InP HPT-based monolithic oscillator and a low-cost E/O converter made up of two LDs, has been proposed. In the proposed scheme, the monolithic oscillator performs O/E conversion as well as electrical free-running oscillation and two low-speed LDs carried out the E/O

conversion, resulting in the compact and cost-effective configuration.

Although both two schemes successfully demonstrated single-mode oscillation with SMSR larger than 50 dB by controlling self-injection power, the following two things should be more considered in future works.

One of them is that the SMSR should be more increased without degradation of output phase noise. It will be realized by adding an additional optical delay line having different length like a dual-loop OEO [11].

The other is to optimize the electrical-loop gain and the optical-loop loss for achieving large SMSR as well as low phase noise. In this initial demonstration, the only optical-loop loss was controlled by adjusting an optical attenuator with the electrical-loop gain fixed to obtain the large SMSR. However, there will be optimum values of electrical gain and optical loss to achieve both low output phase noise and large SMSR, if the sum of them is constant. It will be more considered in the future work.

In the following chapter, millimeter-wave fiber-fed wireless systems will be proposed and demonstrated as one of applications of the optoelectronic SIL oscillator.

## **Chapter 5**

# **60-GHz Fiber-Fed Wireless Systems Based on Optoelectronic SIL Oscillators**

### **5-1. Introduction**

In this chapter, a 60-GHz fiber-fed wireless system based on the proposed optoelectronic self-injection-locked (SIL) oscillator is introduced and experimentally demonstrated. In the proposed system, the optoelectronic SIL oscillator is installed in a central station and performs optical up-conversion of low frequency data signals as well as generation of low phase-noise optical local oscillator (LO) signals.

With this method, the 5MS/s 8-PSK data is successfully transmitted along 10-km fiber-optic and 1.5-m 60-GHz wireless links. In addition, the system performance dependent on LO signal's phase noise, which is controlled by the self-injection power, is analyzed and the optimal self-injection power is determined.

### ***5-1-1. Great interest in 60 GHz***

With the help of wireless technology development, we are using mobile phones anywhere, having wireless local area network (LAN) services in many hot spots, and watching television programs in public places through the digital media broadcasting receivers. Moreover, the prevailing wireless systems are evolving to the triple play systems providing voice, data, and video services at the same time.

In order to realize such systems, millimeter-wave systems have been actively investigated. In particular, 60-GHz systems have been considered as a most promising candidate due to following advantages.

- **License-free:** Several gigahertz bandwidths are opened at 60-GHz band in many countries and they are license-free band [27-29].
- **High free-space loss of 10-15 dB/km:** The 60-GHz band can be used for short range communications such as indoor wireless systems requiring less interference among users. In addition, such high loss characteristics can be applied to frequency reuse in wireless systems having lots of cells [30].
- **High directivity:** The 60-GHz band has high-directivity gain

and that is very useful to increase the transmission length, to decrease signal interferences, and to mitigate inter-symbol-interferences caused by multi-path fading.

- **Short wavelength:** It is possible to design small system components.

Because of the above advantages, lots of applications of 60 GHz have been proposed and demonstrated in various research fields such as wireless systems or imaging and sensor systems.

### ***5-1-2.60-GHz fiber-fed wireless systems***

60 GHz is a promising candidate for realization of future broadband wireless communication systems. However, there are some problems to realize 60-GHz systems. As mentioned in the previous section, the free-space loss of 60 GHz is very high, so that a lot of base stations covering small-sized cells are required to implement systems. Moreover, high speed millimeter-wave devices based on compound semiconductors are very expensive and high frequency component designs and packages are also difficult. Therefore, the deployment cost of 60-GHz systems will be very high and the design of simple and cost-effective base stations becomes important. As one solution, fiber-fed wireless systems have been attracting much attention [31-33].

Fig. 5-1 shows the schematic of simple fiber-fed wireless systems. In the systems, radio signals are converted to optical signals by electrical-to-optical (E/O) converters and delivered to base stations from central stations, resulting in low loss transmission of radio signals via optical fiber. Therefore, for 60-GHz signals suffering high attenuation in free space, this fiber-fed wireless system can extend transmission distance. In addition, the direct optical transmission of radio signals can help reducing complex and expensive devices at many base stations, and it

can induce easy control of many base stations with one central station. In case of down link data transmission, radio signals are generated by only optical-to-electrical (O/E) conversion process at the base stations and the generated radio signals are transmitted to mobile users after simple electrical amplification, resulting in very simple base station architectures. Fig. 5-2 conceptually shows the advantage of fiber-fed wireless systems.

However, the system requires a millimeter-wave phase-locked oscillator for generation of low phase-noise LO signal which is needed for up-conversion of the wireless data signals into the desired millimeter-wave bands. When phase-modulated wireless signals such as phase-shift keying data signals are up-converted to the desired bands, the LO signal's phase noise is key parameter to determine the quality of the up-converted data signals. As the LO signal has lower phase noise, the phase error in the up-converted data signals becomes lower.

In practical, phase-locked oscillators generating low phase-noise signals at millimeter-wave bands are very expensive and it is hard to realize it. A new configuration without RF phase-locked oscillators in the central station will be proposed in the following section.

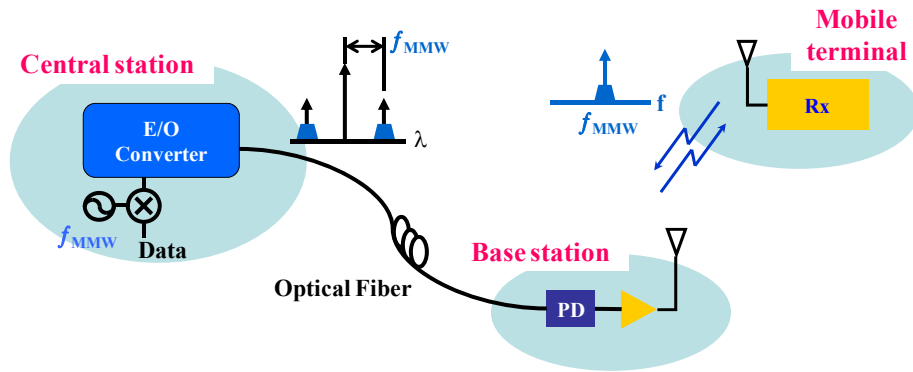


Fig. 5-1. Simple configuration for fiber-fed wireless systems.

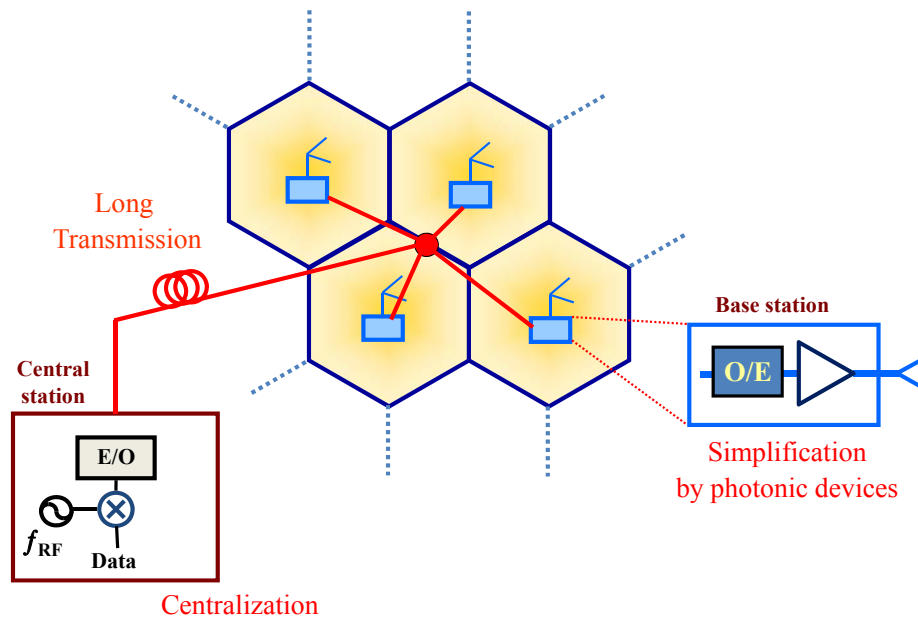


Fig. 5-2. Advantages of fiber-fed wireless systems.

## **5-2. Fiber-fed wireless system based on an optoelectronic SIL oscillator**

### ***5-2-1. Operation principle of LO signal generation and up-conversion***

Fig. 5-3 shows the proposed fiber-fed wireless system using an optoelectronic self-injection-locked (SIL) oscillator instead of an RF phase-locked oscillator in the central station. The optoelectronic oscillator generates optical local oscillator (LO) signals modulated by a low phase-noise millimeter-wave signal and performs optical up-conversion.

As shown in the figure, a commercially available 10-Gb/s distributed feedback laser diode (DFB LD) is directly modulated by a electrical LO signal, which is the output from the free-running oscillator oscillating at 30-GHz band, and data signals carried by intermediate frequency (IF), and generates several optical sidebands. The optical sidebands are separated by LO frequency ( $f_{LO}$ ) and IF ( $f_{IF}$ ) from the optical carrier. Other optical sidebands are also produced separated by  $f_{LO} \pm f_{IF}$  from the optical carrier because of the nonlinear characteristics of the DFB LD.

Theses optical signals are injected into the second DFB LD along an

optical circulator. As mentioned in Ch. 4, the only sidebands located at the longer (or shorter) wavelength receive optical gain by the second LD. The output signals from the second LD are amplified by an optical amplifier and divided into two paths by an optical splitter.

The one path is connected to the free-running oscillator through 2.4-km long single-mode fiber. The optical signals following this route are converted to a 30-GHz electrical signal by an O/E converter and lock the free-running oscillator, resulting in self-injection locking for output phase-noise reduction. The self-injection power was controlled by an optical attenuator.

The other path is connected to a base station via 10-km long single-mode fiber. In a base station, electrical up-converted data signals are generated at the desired 60-GHz band corresponding to the 2<sup>nd</sup> harmonic of the optoelectronic SIL oscillation frequency by beating of optical sidebands in a photo diode, as shown in Fig. 5-3.

The generated data signals are amplified and radiated to a mobile terminal through an antenna, and the radiated signals are received and down-converted for the data evaluation at a mobile terminal.

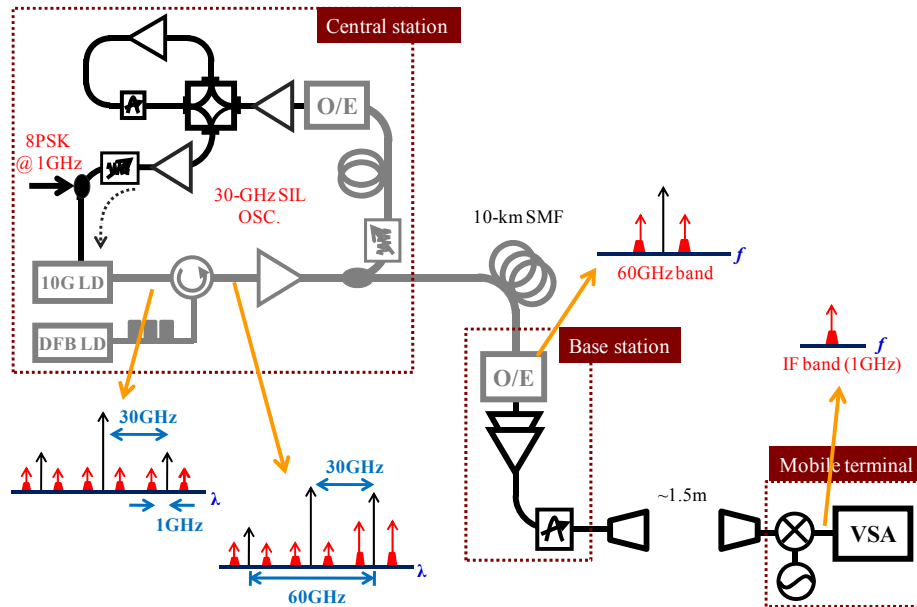


Fig. 5-3. 60-GHz fiber-fed wireless system based on an optoelectronic SIL oscillator.

### ***5-2-2. Experimental results for LO signal generation***

The experimental setup for demonstration of 60-GHz fiber-fed wireless system based on optoelectronic SIL oscillator is shown in Fig. 5-3.

The optoelectronic SIL oscillator used for this demonstration was same as the proposed one in chapter 4. All electrical components for the optoelectronic SIL oscillator operated at a 30-GHz band and the free-running oscillator was composed of a low noise amplifier (LNA), a band-pass filter having  $Q$  of 100, and 4-port 3-dB coupler for the signal injection and extraction.

First of all, the optical spectra of the output signals from directly modulated DFB LD and the second DFB LD with optical injection of the modulated optical signals were measured and Fig. 5-4 shows the results. From Fig. 5-4 (b), it can be shown that the only optical sideband located at the longer wavelength was amplified by the second DFB LD.

These optical signals were detected by a high-speed photo diode (PD) having 3-dB bandwidth of 60 GHz and a LO signal was obtained. Fig. 5-5 shows RF spectra of obtained 1<sup>st</sup> and 2<sup>nd</sup> harmonic (60 GHz) LO signals according to the self-injection power level. When the 2<sup>nd</sup>

harmonic LO signals were measured, two LNAs having total gain of about 52 dB were used. As expected, the signal quality is improved with increasing the injection power, but the undesired side modes are also increased. The side modes will degrade the system performance and it will be discussed in the next section.

Fig. 5-6 shows the phase noises of the fundamental and 2<sup>nd</sup> harmonic LO signals measured at 10-kHz frequency offset from the oscillation frequency with different injection power level. The phase noise becomes lower with higher injection power level. The phase-noise degradation (about 6~7 dB) of 2<sup>nd</sup> harmonic LO signal, as compared with the fundamental value, agrees well with the theoretical value of 6 dB [34].

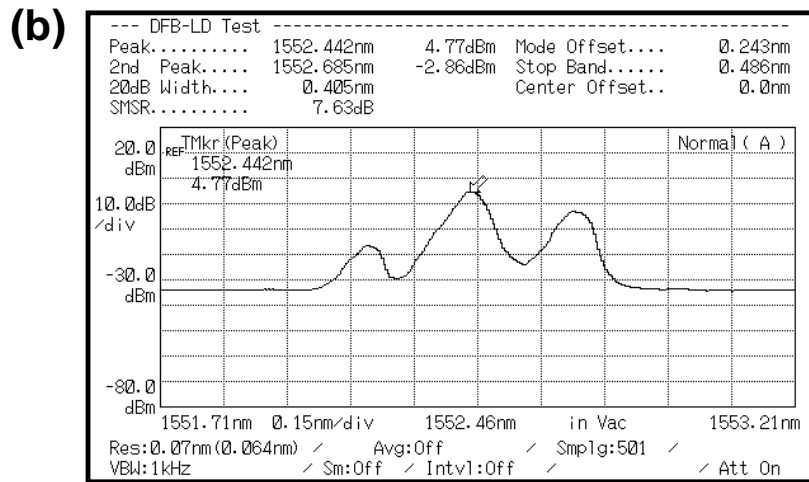
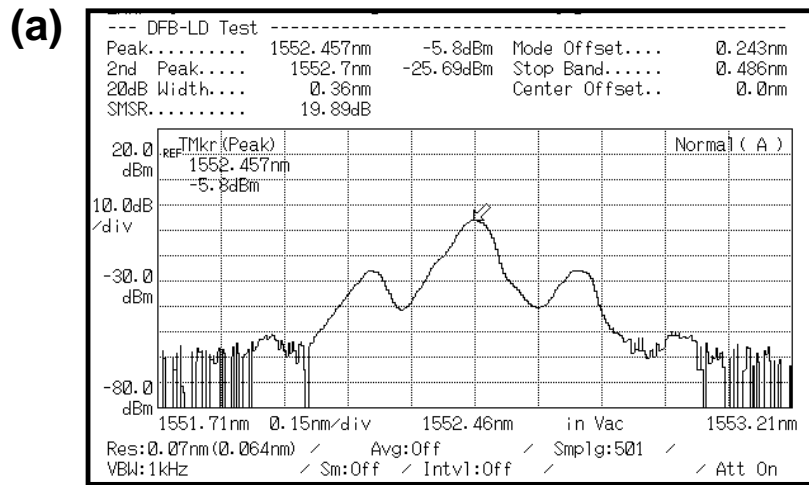


Fig. 5-4. Measured optical spectra of output signals from (a) directly modulated DFB LD and (b) the second DFB LD with optical injection of the modulated optical signals.

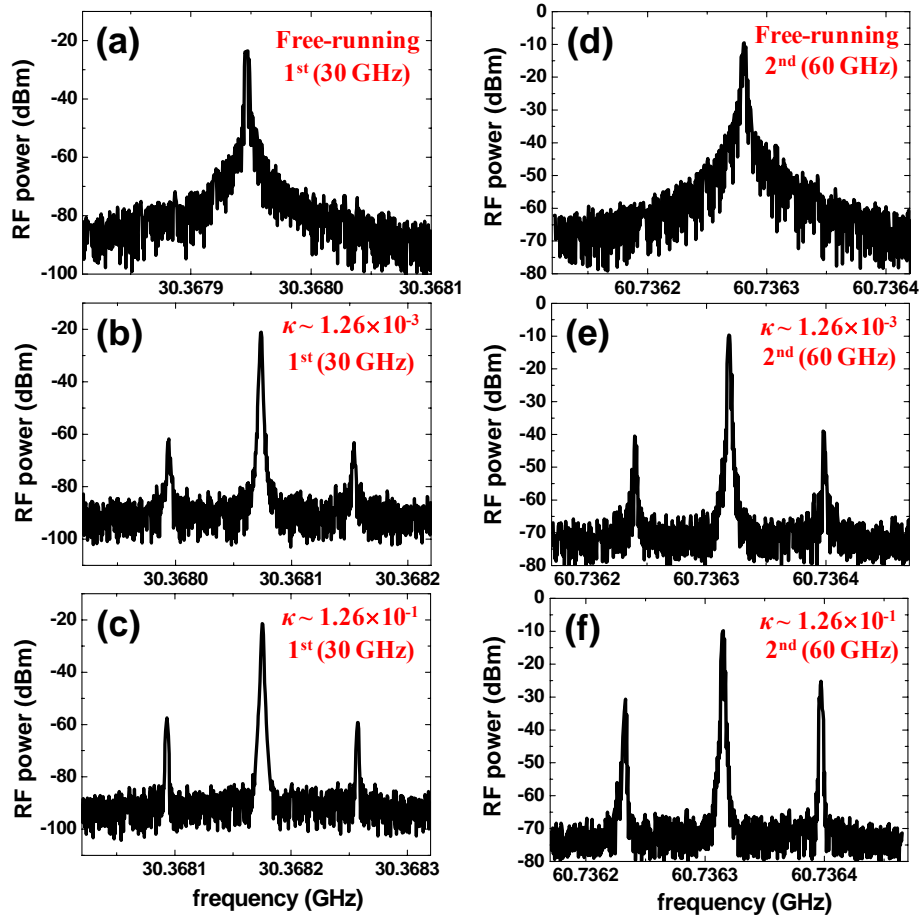


Fig. 5-5. Generated 1<sup>st</sup> and 2<sup>nd</sup> harmonic LO signals according to the self-injection power level ( $\kappa$ ).

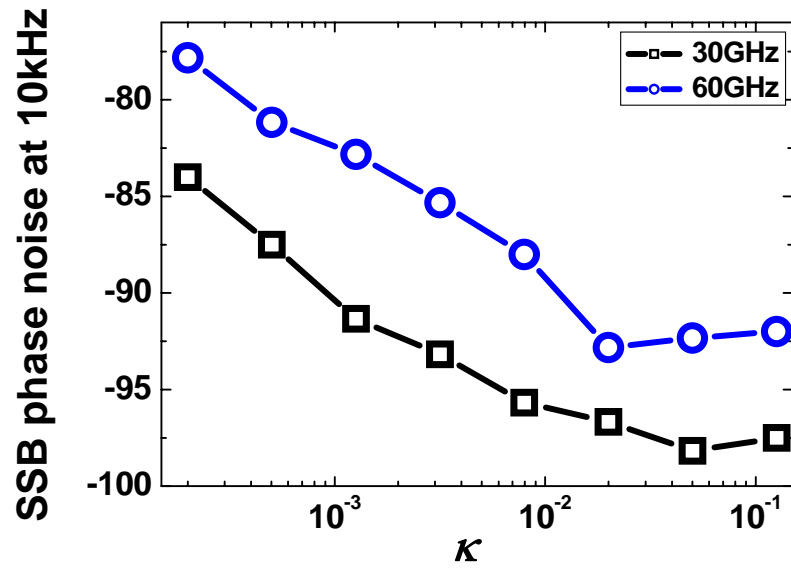


Fig. 5-6. Measured phase noises of 1<sup>st</sup> (30 GHz) and 2<sup>nd</sup> (60 GHz) LO signals with increasing self-injection power level ( $\kappa$ ).

### ***5-2-3. Demonstration of data transmission along fiber and 60-GHz wireless links***

For demonstration of data transmission in a fiber-fed wireless system, the 5MS/s 8-PSK data signals carried by  $f_{IF}$  of 1 GHz were injected into the DFB LD with the LO signal generated by the optoelectronic SIL oscillator, as shown in Fig. 5-3.

The optical signals modulated by LO and data signals were transmitted to a base station via 10-km optical fiber and detected by a high-speed PD and the detected signals are shown in Fig. 5-7. The up-converted upper sideband (USB) and lower sideband (LSB) data signals were obtained along the 2<sup>nd</sup> harmonic LO signal. The result was measured with the fixed self-injection power level of about  $1.26 \times 10^{-3}$ .

Among the up-converted data signals, the only USB data signals were selected by a band-pass filter and radiated to a mobile terminal through an antenna. In the mobile terminal, the radiated signals were received and down-converted to lower frequency band. Finally, the down-converted data were demodulated and evaluated by a vector signal analyzer (VSA).

The incoming digital data signals have their original vector positions in complex domain and the VSA provides the discrepancy information

between the original vector positions and the demodulated-signal's vector positions in the form of error vector magnitude (EVM).

The constellation and eye diagram of the demodulated 5MS/s 8-PSK data signal obtained by the VSA are shown in Fig. 5-8 (a) and (b), respectively. The low EVM of about 6.27% corresponding to the signal-to-noise (SNR) ratio of about 24.0 dB was obtained at the fixed self-injection power level of about  $1.26 \times 10^{-3}$ .

The constellation and eye diagram according to LO signal's phase noise characteristic were also measured and the results are shown in Fig. 5-9. The phase-noise characteristic was controlled by the self-injection power level. From the figure, the phase error of the demodulated data was reduced by the weak self-injection power level ( $\kappa \sim 1.26 \times 10^{-3}$ ) from 5.25 % to 2.85 % since the LO signal's phase noise was reduced by self-injection locking as shown in Fig. 5-6. However, the system performance was deteriorated at the strong self-injection power level of  $\kappa \sim 1.26 \times 10^{-1}$  (Fig. 5-6 (c)). It is because that the undesired side modes are generated along the LO signal and their power is increased with the self-injection power, causing low SNR.

Fig. 5-10 shows the EVM of the 5MS/s 8-PSK data signal demodulated by a VSA with increasing the self-injection power level ( $\kappa$ ). Even if the self-injection power is low, the self-injection locking

can be achieved, resulting in generation of low phase-noise LO signal as compared with the free-running case. The lower phase noise induces the lower phase error and that results in lower EVM value. However, the EVM value increases with the self-injection power level ( $\kappa$ ) since the SNR decreases due to the unwanted side modes generated along LO signal. Fig. 5-10 indicates that  $\kappa$  should be lowered than about  $4.5 \times 10^{-2}$  for obtaining the system performance better than free-running case.

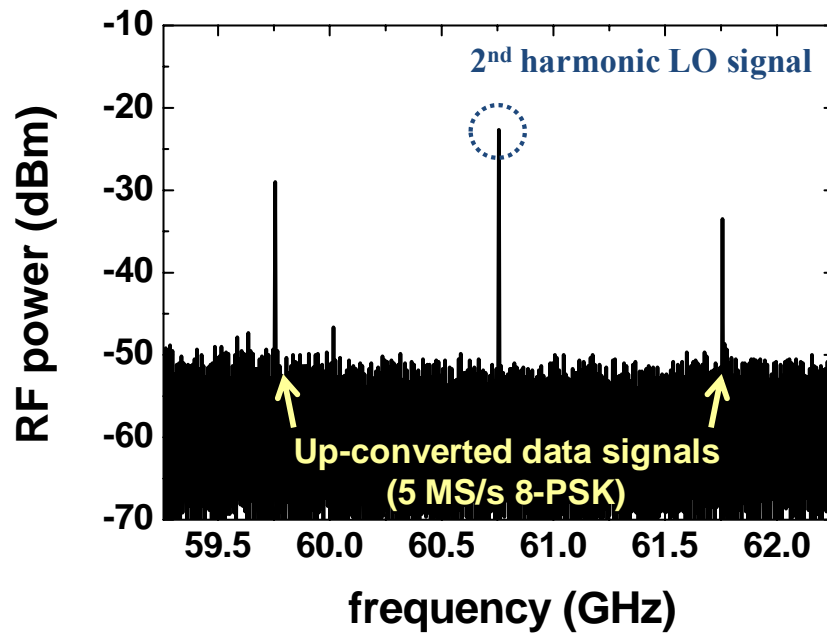


Fig. 5-7. 5MS/s 8-PSK data signals up-converted to the 60-GHz band.

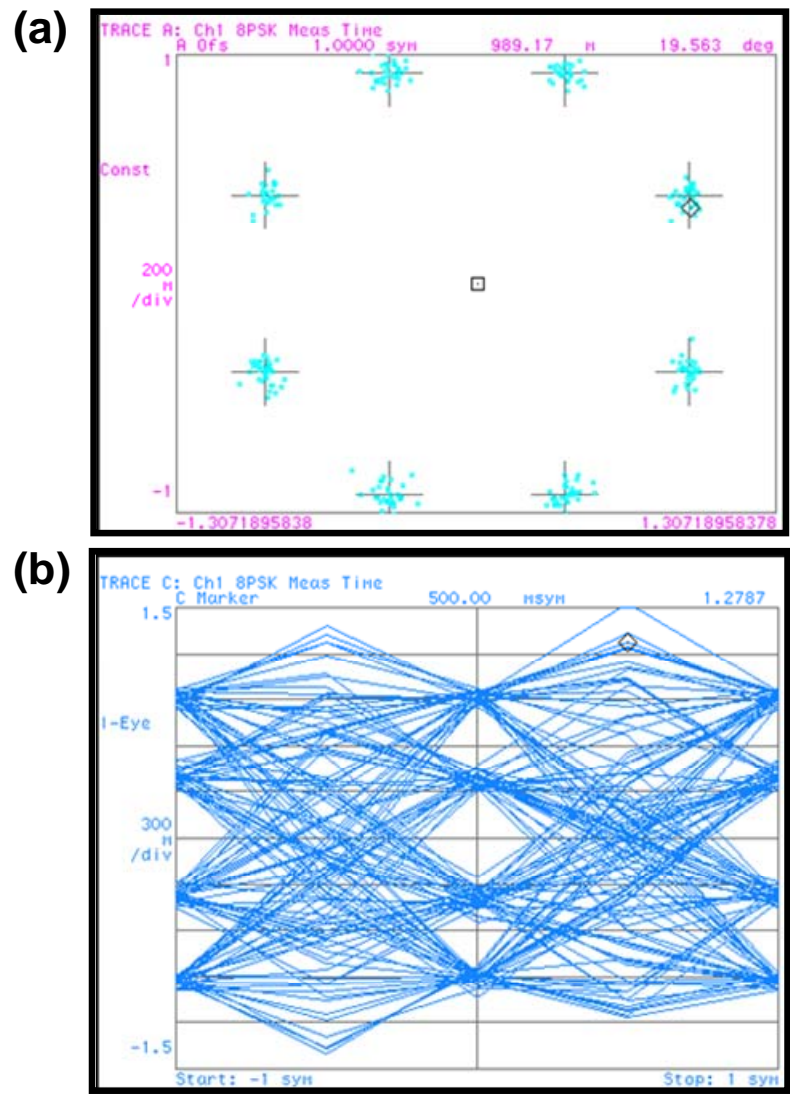


Fig. 5-8. Constellation and eye diagram of the demodulated 5 MS/s 8-PSK data signals.

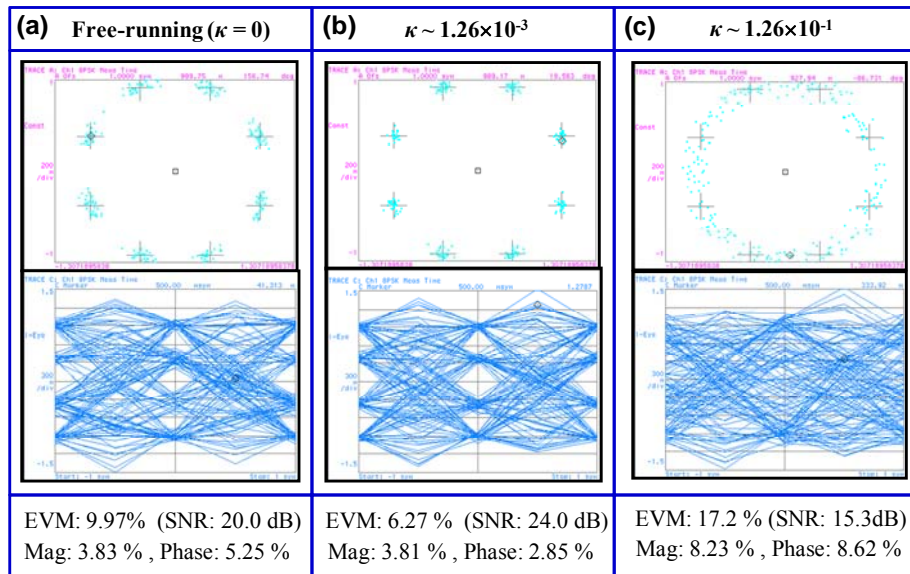


Fig. 5-9. Measured constellation and eye diagram of the demodulated 5 MS/s 8-PSK data signals according to the self-injection power level ( $\kappa$ ).

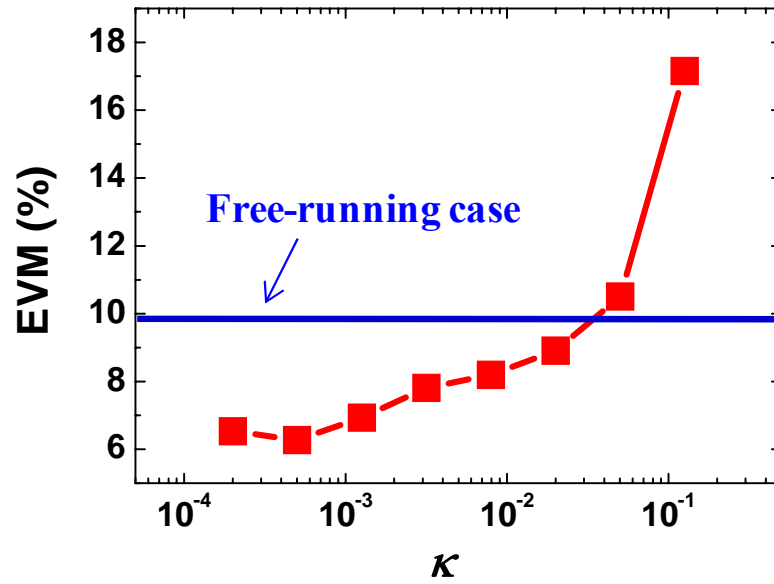


Fig. 5-10. Measured EVM of the demodulated 5 MS/s 8-PSK data signals as a function of self-injection power level ( $\kappa$ ).

### 5-3. Conclusions

A new 60-GHz fiber-fed wireless system based on an optoelectronic self-injection-locked (SIL) oscillator has been proposed. In the proposed fiber-fed wireless system, the optoelectronic SIL oscillator performed generation of low phase-noise local oscillator (LO) signal and optical up-conversion at the same time.

With the proposed scheme, 5 MS/s 8-PSK data carried by 1-GHz intermediated frequency (IF) were successfully transmitted along 10-km long single-mode fiber and about 1.5-m 60-GHz wireless channel. The measured error vector magnitude (EVM) was 6.27 % corresponding to the signal-to-noise ratio (SNR) of 24.0 dB at the self-injection power level of  $1.26 \times 10^{-3}$ . Moreover, the system performance which depends on LO signal quality was investigated.

Unlike the previous systems, our scheme doesn't need a high speed and high cost RF phase-locked oscillator at a central station. In our initial demonstration, the used optoelectronic SIL oscillator was somewhat bulky since the free-running oscillator and optical-to-electrical converter were realized by independent modules, but it can be compact and cost-effective by using monolithic microwave integrated circuit (MMIC) technology, as shown in Fig. 5-11.

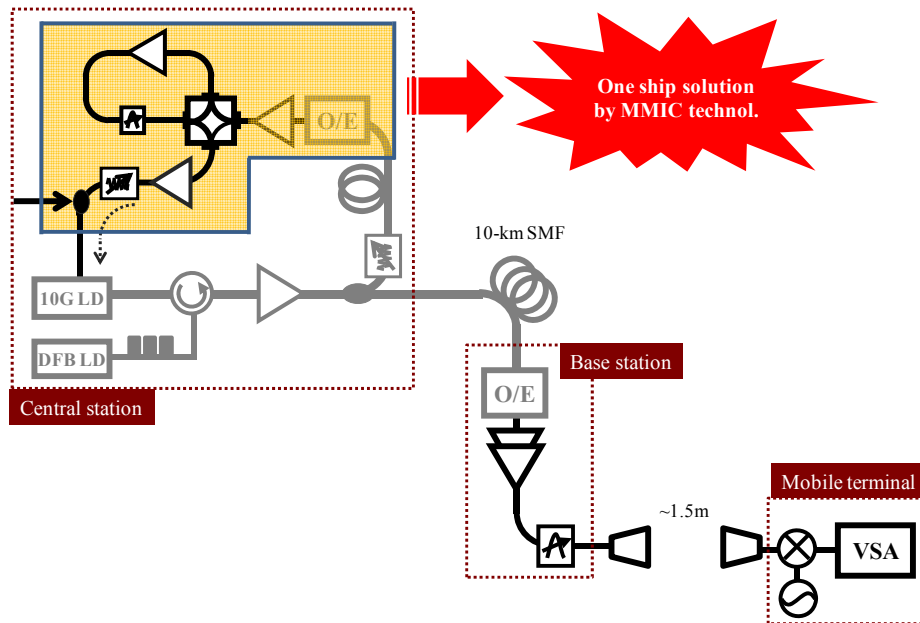


Fig. 5-11. Simple fiber-fed wireless system based on an optoelectronic SIL oscillator.

## Chapter 6

### Summary

In most of wireless communication systems using phase-modulated data signals for enhancing bandwidth efficiency, the phase-noise characteristic of a local oscillator (LO) is one of key parameters to determine the system performance. It is because the lower phase error can be obtained with the lower phase-noise LO signal.

The stable and low phase-noise oscillators can be realized by using a high quality-factor ( $Q$ ) external resonator. However, it is hard to realize high- $Q$  devices especially in higher frequency bands such as millimeter-wave bands. In order to overcome the above problem, several types of optoelectronic oscillators using an optical delay line as a high- $Q$  external resonator have been investigated, but they are bulky and expensive.

In this dissertation, new optoelectronic oscillators (OEOs) for generation of low phase-noise signals with a simple configuration were proposed and demonstrated.

Chapter 2 explained and compared the conventional methods for generation of OEOs. Several types of OEOs have been proposed for realization of single-mode oscillation with ultra low phase noise.

Among them, a dual-loop OEO is most promising to achieve low phase noise and single-mode oscillation at the same time since it can provide low phase noise with a long loop and the high side-mode suppression ratio (SMSR) with a short loop. However, two loops are coupled to each other, limiting the increase of SMSR.

The two new OEOs were proposed, experimentally demonstrated, and compared over the chapter 3 and 4.

In chapter 3, a hybrid injection-locked OEO for single-mode oscillation was proposed. The proposed OEO was composed of an electrical oscillator and a single-loop OEO. By injecting OEO modes into an electrical oscillator, it extracted a desired mode from multiple modes in an OEO. Although the phase noise is degraded about 6 dB at 10-kHz frequency offset by injection-locking, extraction of a desired mode among injected OEO modes separated by about 84 kHz at 30-GHz bands can be successfully demonstrated. However, the proposed scheme cannot produce the optical signal modulated by the generated high spectral-purity electrical signal since an electrical oscillator is used as the slave oscillator.

Chapter 4 introduced an optoelectronic self-injection-locked (SIL) oscillator, where a part of the electrical output signal is self-injected after passing through a long optical delay line for output phase-noise

reduction. Unlike typical OEOs, the optical loop worked as a passive feedback loop. With this SIL oscillator, the single-mode oscillation at 30-GHz bands with SMSR of 50 dB and output phase-noise reduction of about 18 dB at 10-kHz frequency offset were experimentally demonstrated. In addition, more compact and cost-effective configuration for the SIL oscillator composed of an InP HPT-based monolithic oscillator and an electrical-to-optical converter realized by two low-speed and low-cost laser diodes was proposed and experimentally demonstrated at 10-GHz bands.

Finally, a 60-GHz fiber-fed wireless system based on the optoelectronic SIL oscillator was proposed in chapter 5. In the proposed system, the optoelectronic SIL oscillator carried out low phase-noise local oscillator (LO) signal generation and optical up-conversion, simultaneously. 5MS/s 8-PSK data signals are successfully transmitted along 10-km fiber-optic and about 1.5-m 60-GHz wireless links. In addition, the system performance to depend on phase noise of a LO signal was investigated.

In this dissertation, the low phase-noise signal was generated by the proposed optoelectronic SIL oscillator and it was used as a LO signal for up-conversion of data signals into the desired band in a 60-GHz fiber-fed wireless system. Although the only fiber-fed wireless system

was introduced and demonstrated as an application of the optoelectronic SIL oscillator, it was believed that the proposed oscillator is very useful for other applications such as optical analog-to-digital converters since it can generate optical signals as well as micro-/millimeter wave signals.

## Bibliography

- [1] David M. Pozar, *Microwave Engineering*, John Wiley & Sons, Ch. 12, 2005.
- [2] Behzad Razavi, *RF Microelectronics*, Printice Hall, Ch. 7, 1998.
- [3] Thomas H. Lee, and A. Hajimiri, "Oscillator phase noise: A tutorial," *IEEE J. Solid-State Circuits*, vol. 35, no. 3, pp. 326-336, Mar. 2000.
- [4] M. Kaba, H. -W. Li, A. S. Daryoush, J. -P. Vilcot, D. Decoster, J. Chazelas, G. Bouwmans, Y. Quiquempois, and F. Deborgies, "Improving thermal stability of opto-electronic oscillators," *IEEE Microw. Mag.*, Vol. 7, no. 4, pp. 38-47, Aug. 2006
- [5] X. S. Yao and L. Maleki, "Optoelectronic microwave oscillator," *J. Opt. Soc. Am. B.*, vol. 13, no. 8, pp. 1725-1735, Aug. 1996.
- [6] X. S. Yao and L. Maleki, "Converting light into spectrally pure microwave oscillation," *Opt. Lett.*, vol. 21, no. 7, pp. 483-485, Apr. 1996.
- [7] X. S. Yao and L. Maleki, "Optoelectronic oscillator for photonic systems," *IEEE J. Quantum Electron.*, vol. 35, no. 18, pp. 1554-1555, Sep. 1999.
- [8] Yu Ji, X. S. Yao and L. Maleki, "Compact optoelectronic oscillator with ultra phase noise performance," *Electronics Letters*, vol. 29, no. 15, pp. 134-1343, July. 1993.
- [9] D. Eliyahu and L. Maleki, "Low phase noise and spurious level in multi-loop opto-electronic oscillators," *Proc. 2003 IEEE Int. Frequency Control Symp.*, 2003, pp. 405-410.
- [10] D. Eliyahu, K. Sariri, M. Kamran, and L. Maleki, "Improving short and

- long term frequency stability of the opto-electronic oscillator,” *Proc. 2002 IEEE Int. Frequency Control Symp.*, 2002, pp. 580-583.
- [11] X. S. Yao and L. Maleki, “Multiloop optoelectronic oscillator,” *IEEE J. Quantum Electron.*, vol. 36, no. 1, pp. 79-84, Jan. 2000.
- [12] W. Zhou, and G. Blasche, “Injection-locked dual optoelectronic oscillator with ultra-low phase noise and ultra-low spurious level,” *IEEE Transaction on Microwave Theory and Techniques*, vol. 53, no. 3, pp. 929-933, Mar. 2005.
- [13] H. C. Chang, X. Cao, M. J. Vaughan, U. K. Mishra, and R. A. York, “Phase noise in externally injection-locked oscillator array,” *IEEE Transaction on Microwave Theory and Techniques*, vol. 45, no. 11, pp. 2035-2041, Nov. 1997.
- [14] K. Kurokawa, “Injection locking of microwave solid-state oscillator,” *Proc. IEEE*, vol. 61, no. 10, pp. 1386-1410, Oct. 1973.
- [15] K. -H. Lee, J. -Y. Kim, and W. -Y. Choi, “Single-mode extraction using injection-locking in opto-electronic oscillators,” *submitted for publication to Opt. Lett.*, 2007.
- [16] R. Adler, “A study of locking phenomena in oscillators,” *Proc. IRW*, vol. 34, no. 6, pp. 351-357, June 1946.
- [17] K. Kurokawa, “Noise in synchronized oscillators,” *IEEE Trans. Microw. Theory Tech.*, vol. 16, no.4, pp. 234-240, April 1968.
- [18] H.-C. Chang, “Stability analysis of self-injection-locked oscillators,” *IEEE Trans. Microw. Theory Tech.*, vol. 51, no. 9, pp.1989-1993, Sep. 2003.
- [19] H.-C. Chang, “Phase Noise in self-injection-locked oscillators,” *IEEE Trans. Microw. Theory Tech.*, vol. 51, no. 9, pp.1994-1999, Sep. 2003.

- [20] T. -P. Wang, Z. -M. Tsai, K. -J. Sun, and H. Wang, "Phase-noise reduction of X-band push-push oscillator with second-harmonic self-injection techniques," *IEEE Trans. Microw. Theory Tech.*, vol. 55, no.1, pp.66-77, Jan. 2007.
- [21] F. Kuroki, S. Ishikawa, T. Yoneyama, "Comparative study on two types of self-injection locked NRD guide gunn oscillators," in *Proc. European Microw. Conf.*, 2005.
- [22] K. -H. Lee, J. -Y. Kim, and W. -Y. Choi, "A 30-GHz self-injection-locked oscillator having a long optical delay line for phase-noise reduction," *accepted for publication to IEEE Photonics Technology Letters*, 2007.
- [23] U. Gliese, S. Norskov, and T. N. Nielsen, "Chromatic dispersion in fiber-optic microwave and millimeter-wave links," *IEEE Trans. Microw. Theory Tech.*, vol. 44, no. 10, pp. 1716–1724, Oct. 1996.
- [24] H. -S. Ryu, Y. -K. Seo, and W. -Y. Choi, "Dispersion-tolerant transmission of 155-Mb/s data at 17 GHz using a 2.5-Gb/s-Grade DFB laser with wavelength-selective gain from an FP laser diode," *IEEE Photon. Technol. Lett.*, vol. 16, no. 8, pp. 1942–1944, Aug. 2004.
- [25] H. -Y. Ryu, *Optical single sideband modulation using a semiconductor laser under modulation light injection*, M. S. dissertation, Dept. Electr. Electron. Eng., Yonsei Univ., Seoul, Korea, 2004.
- [26] H. Kamitsuna, T. Shibata, K. Kurishima, and M. Ida, "Direct optical injection-locking of InP/InGaAs HPT oscillator ICs for microwave photonics and 40Gbps-class optoelectronic clock recovery." *IEEE Trans. Microw. Theory Tech.*, vol. 50, no. 12, pp.3002-3008, Dec. 2002.
- [27] J. Mikkonen, C. Corrado, C. Evcı, and M. Prögler, "Emerging wireless

- broadband networks,” *IEEE Commun. Mag.*, pp. 112-117, Feb. 1998.
- [28] H. Izadpanah, “A millimeter-wave broadband wireless access technology demonstrator for the next-generation internet network reach extension,” *IEEE Commun. Mag.*, pp. 140-145, Sep. 2001.
- [29] P. Smulders, “Exploiting the 60 GHz band for local wireless multimedia access: prospects and future directions,” *IEEE Commun. Mag.*, pp. 140-147, Jan. 2002.
- [30] M. Marcus and B. Pattan, “Millimeter wave propagation: spectrum management implications,” *IEEE Microwave Mag.*, pp. 54-62, Jun. 2005.
- [31] A. J. Seeds, “Microwave photonics,” *IEEE Trans. Microw. Theory Tech.*, vol. 50, no. 3, pp. 877-887, Mar. 2002.
- [32] H. Ogawa, D. Polifko, and S. Banda, “Millimeter-wave fiber-optics systems for personal radio communication,” *IEEE Trans. Microw. Theory Tech.*, vol. 40, no.12, pp.2285-2293, Dec.1992.
- [33] G. H. Smith, D. Novak, and C. Lim, “A millimeter-wave full duplex fiber-radio star-tree architecture incorporating WDM and SCM,” *IEEE Trans. Microw. Theory Tech.*, vol. 10, no.10, pp.1650-1652, Nov.1998.
- [34] J. S. Lee, H. –J. Song, W. B. Kim, M. Fujise, Y. –H. Kim and J. –I. Song, “All-optical harmonic frequency upconversion of radio over fiber signal using cross-phase modulation in semiconductor optical amplifier,” *IEE Electron. Lett.*, vol. 40, no. 19, pp.1211-1213, September 2004.

## Publication Lists

### *International Journals*

- [1] **Kwang-Hyun Lee**, Jae-Young Kim, Woo-Young Choi, Hideki Kamitsuna, Minoru Ida, and Kenji Kurishima “Low-cost optoelectronic self-injection-locked oscillators,” submitted for publication in *IEEE Photon. Technol. Lett.*.
  
- [2] **Kwang-Hyun Lee**, Jae-Young Kim, and Woo-Young Choi, “A 30-GHz self-injection-locked oscillator having a long optical delay line for phase-noise reduction,” *IEEE Photon. Technol. Lett.*, vol. 19, no. 24, pp. 1982-1984, 2007.
  
- [3] **Kwang-Hyun Lee** and Woo-Young Choi, “Harmonic signal generation and frequency up-conversion using selective sideband Brillouin amplification in single-mode fiber,” *Opt. Lett.*, vol. 32, no.12, pp. 1686-1688, 2007.
  
- [4] **Kwang-Hyun Lee**, Woo-Young Choi, Young-Ahn Leem, Kwang-Seong Choi, and Kyung-Hyun Park, “Harmonic signal generation and frequency up-conversion using a hybrid mode-locked multi-section DFB laser,” *IEEE Photon. Technol. Lett.*, vol. 19, no. 12, pp. 901-903, 2007.
  
- [5] **Kwang-Hyun Lee**, Woo-Young Choi, Young-Ahn Leem, and Kyung-

Hyun Park, "Harmonic millimeter-wave generation and frequency up-conversion using a passively mode-locked multi-section DFB laser under external optical injection," *IEEE Photon. Technol. Lett.*, vol. 19, no. 3, pp. 161-163, 2007.

- [6] ***Kwang-Hyun Lee***, Young-Min Jhon, and Woo-Young Choi, "Photonic phase shifter based on a vector-sum technique with polarization maintaining fibers," *Opt. Lett.*, vol. 30, no. 7, pp. 702-704, 2005.
- [7] ***Kwang-Hyun Lee***, Woo-Young Choi, Sang-Su Choi, and Kyung-Whan Oh, "A novel fiber-optic microwave filter using multimode DCF," *IEEE Photon. Technol. Lett.*, vol. 15, no. 7, pp. 969-971, 2003.
- [8] ***Kwang-Hyun Lee***, Young-Sang Cho, Sangin Kim, and Woo-Young Choi, "A tunable-output wavelength converter based on a self-seeded Fabry-Perot laser diode with a chirped fiber grating," *Microwave Opt. Technol. Lett.*, vol. 37, no. 7, pp. 35-36, 2003.

### ***International Conferences***

- [1] Myung-Jae Lee, Hyu-Soon Kang, ***Kwang-Hyun Lee***, and Woo-Young Choi, "Fiber-fed 60-GHz self-heterodyne systems using self-oscillating harmonic optoelectronic mixers based on CMOS-compatible APDs" submitted for publication in *IEEE MTT-S International Microwave Symposium Photon. Technol. Lett.*, 2008.

- [2] **Kwang-Hyun Lee**, Jae-Young Kim, and Woo-Young Choi, "Hybrid dual-loop optoelectronic oscillators," *International Topical Meeting on Microwave Photonics 2007*, pp. 74-77, Oct. 3-5, 2007, Victoria, Canada.
- [3] **Kwang-Hyun Lee**, Woo-Young Choi, Young-Ahn Leem, Kwang-Seong Choi, and Kyung-Hyun Park, "Harmonic frequency up-conversion based on actively mode-locked multi-section DFB lasers for 60 GHz Radio-on-Fiber systems," *Asian-Pacific Microwave Photonics conference 2007*, pp. 151-153 April 25-27. 2007, Jeju Island, Korea.
- [4] **Kwang-Hyun Lee**, and Woo-Young Choi, "Millimeter-wave harmonic frequency up-conversion using selective sideband Brillouin amplification," *OFC 2007*, OWN6, March 25-29, 2007, Anaheim, USA.
- [5] **Kwang-Hyun Lee**, Woo-Young Choi, Young-Ahn Leem, and Kyung-Hyun Park, "All optical harmonic frequency up-converters based on self-pulsating multi-section DFB lasers for 60 GHz RoF down link systems," *Asia-Pacific Microwave Photonics Conference 2006*, C-38, April. 2006, Kobe, Japan.
- [6] **Kwang-Hyun Lee**, Young-Min Jhon, and Woo-Young Choi, "A millimeter-wave photonic vector-sum phase shifter using polarization maintaining fibers," *International Topical Meeting on Microwave Photonics 2004*, pp. 56-59, Oct. 4-6, 2004, Ogunquit, USA.
- [7] **Kwang-Hyun Lee** and Woo-Young Choi, "A Novel photonic vector-

sum phase shifter using polarization maintaining fibers,” *The 5th Japan-Korea Joint Workshop on Microwave and Millimeter-wave Photonics 2004*, pp. 155-158 Jan. 29-30, 2004, Otsu, Shiga, Japan.

- [8] **Kwang-Hyun Lee**, Woo-Young Choi, Sang-Su Choi, and Kyung-Whan Oh, “A tunable fiber-optic microwave filter using multimode DCF,” *The 4th Korea-Japan Joint Workshop on Microwave and Millimeter-wave Photonics 2003*, pp. 37-40 Jan. 23-24, 2003, Daejeon, Korea.

### ***Domestic Conferences***

- [1] **이광현**, 김재영, 최우영, H. Kamitsuna, M. Ida, K. Kurishima “출력 위상 잡음 감쇄를 위한 광전 self-injection-locked 발진기,” *Photonics Conference 2007, FP-6*, 2007년 11월 14-16일, 풍림리조트 (제주도).
- [2] **이광현**, 최우영, “Millimeter-wave harmonic frequency up-conversion using Brillouin amplification,” *Photonics Conference 2006*, pp. 312-313, 2006년 11월 3-5일, 대명콘도(단양).
- [3] **이광현**, 최우영, “Stimulated Brillouin scattering을 이용한 하모닉 밀리미터파 생성 방법,” *13th Conference on optoelectronics and optical communications 2006*, pp. 272-273, 2006년 5월 10-12일, 경남 창원.

- [4] 이광현, 최우영, 임영안, 박경현, “Locking characteristics of self pulsation DFB lasers having active feedback sections,” *Photonics Conference 2005*, pp. 189–190, 2005년 11월 2–4일, 충무 마리나리조트.
- [5] 이광현, 최우영, 임영안, 박경현, “RoF 시스템을 위한 amplified feedback laser 기반의 전광 하모닉 주파수 상향 변환기,” *Photonics Conference 2005*, pp. 13–14, 2005년 11월 2–4일, 충무 마리나리조트.
- [6] 이광현, 최우영, “SOA의 XGM을 이용한 새로운 RF 위상 천이기,” *10th Conference on optoelectronics and optical communications 2003*, pp. 589–590, 2003년 5월 14–16일, 강촌리조트.
- [7] 이광현, 최우영, 최상수, 오경환, “DCF내의 여러모드를 이용한 새로운 tunable fiber-optic microwave filter,” *Photonics Conference 2002*, pp. 253–254, 2002년 10.31–11.1, 용평리조트.
- [8] 이광현, 최우영, 최상수, 오경환, “A novel tunable fiber-optic microwave filter using multi modes in DCF,” *9th Conference on optoelectronics and optical communications 2002*, pp. 221–222, 2002년 5월 16–17일, 경주 교육문화회관.

## ***Patents***

- [1] **이광현**, 최우영, 임영안, 박경현, *밀리미터파 생성 장치 및 그 생성 방법*, 특허등록 (대한민국), 등록번호: 10-0759944, 등록일: 2007년 9월 12일.
  
- [2] **이광현**, 최우영, *편광유지 광섬유를 이용한 벡터성 광 위상천이 및 광 위상천이 방법*, 특허등록 (대한민국), 등록번호: 10-0621049, 등록일: 2006년 8월 30일.
  
- [3] **이광현**, 최우영, *고차모드를 이용한 광 동조 마이크로웨이브 필터*, 특허등록 (대한민국), 등록번호: 10-0428073, 등록일: 2004년 4월 8일, 특허 출원 (해외): PCT/KR03/00518.
  
- [4] **이광현**, 김재영, 최우영, *광전 발전 모드 선택 방법 및 장치*, 특허출원 (대한민국), 출원번호: 10-2007-0080497, 출원일: 2007년 8월 10일.
  
- [5] 강효순, **이광현**, 최우영, *CMOS 구조의 무선 통신 시스템 및 그 제조 방법*, 특허출원, 출원번호: 10-2006-0120683 (대한민국), PCT/KR2007/000928 (해외출원), 출원일: 2006년 12월 1일 (대한민국), 2007년 2월 22일 (해외출원).
  
- [6] **이광현**, 최우영, 임영안, 박경현, *밀리미터파 생성 장치 및 그 생성 방법*, 특허출원, 출원번호: 11/500,646 (미국), 2006-126937 (일본), 출원일: 2006년 3월 10일 (대한민국), 2006년 8월 8일 (미국), 2006년 4월 28일 (일본).

## *Awards*

- [1] TMS Best Paper Award (Bronze Prize): Kwang-Hyun Lee, “Harmonic signal generation and frequency up-conversion using selective sideband Brillouin scattering” *BK21 TMS Institute of Information Technology School of Electrical and Electronic Engineering, Yonsei University, Seoul, Korea.*
  
- [2] 우수 논문상: 이광현, 최우영, “Stimulated Brillouin scattering을 이용한 하모닉 밀리미터파 생성 방법,” 제 13회 광전자 및 광통신 학술 회의, 2006, 부곡 일성 콘도.